Computational antimicrobial peptide design and evaluation against multidrug-resistant clinical isolates of bacteria

Received for publication, July 5, 2017, and in revised form, December 4, 2017 Published, Papers in Press, December 19, 2017, DOI 10.1074/jbc.M117.805499

Deepesh Nagarajan[‡], Tushar Nagarajan[§], Natasha Roy[¶], Omkar Kulkarni[‡], Sathyabaarathi Ravichandran[‡], Madhulika Mishra[‡], Dipshikha Chakravortty[‖], and Nagasuma Chandra[‡**1]**

*From the Departments of [‡]Biochemistry and [§]Computational and Data Sciences, [¶]Molecular Biophysics Unit, [‖]Department of Microbiology and Cell Biology, and **Centre for Biosystems Science and Engineering, Indian Institute of Science (IISc), Bangalore 560012, India*

Edited by Joseph M. Jez

There is a pressing need for new therapeutics to combat multidrug- and carbapenem-resistant bacterial pathogens. This challenge prompted us to use a long short-term memory (LSTM) language model to understand the underlying grammar, *i.e.* the arrangement and frequencies of amino acid residues, in known antimicrobial peptide sequences. According to the output of our LSTM network, we synthesized 10 peptides and tested them against known bacterial pathogens. All of these peptides displayed broad-spectrum antimicrobial activity, validating our LSTM-based peptide design approach. Our two most effective antimicrobial peptides displayed activity against multidrug-resistant clinical isolates of *Escherichia coli*, *Acinetobacter baumannii*, *Klebsiella pneumoniae*, *Pseudomonas aeruginosa*, *Staphylococcus aureus*, and coagulase-negative staphylococci strains. High activity against extended-spectrum β-lactamase, methicillin-resistant *S. aureus*, and carbapenem-resistant strains was also observed. Our peptides selectively interacted with and disrupted bacterial cell membranes and caused secondary gene-regulatory effects. Initial structural characterization revealed that our most effective peptide appeared to be well folded. We conclude that our LSTM-based peptide design approach appears to have correctly deciphered the underlying grammar of antimicrobial peptide sequences, as demonstrated by the experimentally observed efficacy of our designed peptides.

Antibiotic resistance is an ever-increasing threat that is gradually rendering our current repertoire of antibiotics obsolete. If no new drugs are developed, deaths due to antimicrobial resistance are expected to exceed 10 million annually by 2050 (1). Antimicrobial peptides (AMPs)[2] are one potential solution to this problem. Naturally occurring AMPs continue to remain an important component of the innate immune system despite their ancient evolutionary origin and widespread prevalence across many forms of life (2). Some derivatives of these such as pexiganan (3), omiganan (4), and OP-145 (5) are currently undergoing late-stage clinical trials (for diabetic foot ulcers, rosacea, and ear infections, respectively (6)). Other peptides such as novexatin (7) and Lytixar™ (8) are currently undergoing early-stage clinical trials (for the treatment of toenail fungal infections and MRSA, respectively (6)). Currently, over 2000 natural and designed antimicrobial peptides are curated in various databases (9–11) and have displayed broad-spectrum activity against Gram-positive, Gram-negative, fungal, mycobacterial, and protozoal pathogens (9).

Antimicrobial peptides possessing a net positive charge are attracted and incorporated into negatively charged bacterial membranes. Once inside the membrane, they are believed to cause disruption through three possible mechanisms: toroidal pore formation (12), carpet formation (13), and barrel stave formation (14). Although the specifics of each mechanism differ, all propose peptide-induced membrane rupture, allowing cytoplasmic leakage that ultimately leads to death. Recent work has painted a more complex picture of antimicrobial peptide activity. Antimicrobial peptides may also function as metabolic inhibitors (15, 16); inhibitors of DNA (17), RNA (18), and protein synthesis (19); inhibitors of cell wall synthesis (20); and septum formation (21). They are also known to cause ribosomal aggregation (15) and delocalize membrane proteins (22). These effects have only recently begun to receive attention.

Attempts at improving antimicrobial peptides through rational design have been made, resulting in pexiganan (3), leucine-lysine repeats (23), tryptophan-leucine-lysine repeats (24), tryptophan-arginine repeats (25), and structurally nanoengineered antimicrobial peptide polymers (26). These peptides were designed using simple repeating hydrophilic/hydrophobic amino acid motifs with minimal computational input. More sophisticated computational approaches involve optimization and machine-learning algorithms. Genetic algorithms (27), early linguistic models (28), and QSAR-based models (29) have

This work was supported by the Department of Biotechnology (DBT), India. The authors declare that they have no conflicts of interest with the contents of this article.

This article contains Figs. S1–S3, Tables S1–S4, and supporting Datasets S1–S3.

[1] To whom correspondence should be addressed. E-mail: nchandra@iisc.ac.in or sumachandra@gmail.com.

[2] The abbreviations used are: AMP, antimicrobial peptide; MIC, minimum inhibitory concentration; LSTM, long short-term memory; MDR, multidrug-resistant; CoNS, coagulase-negative staphylococcus; MRSA, methicillin-resistant *S. aureus*; ANOVA, analysis of variance; DEG, differentially expressed gene; CGH, comparative genomic hybridization; cfu, colony-forming unit; ESBL, extended-spectrum β-lactamase; MTCC, Microbial Type Culture Collection; DPC, dodecylphosphocholine; MIC, minimum inhibitory concentration; Bi-LSTM, bi-directional LSTM model; MBC, minimum bactericidal concentration; SEM, scanning electron microscopy; MTT, 3-(4,5-dimethylthiazol-2-yl)-2,5-diphenyltetrazolium bromide; SEM, Scanning electron microscopy; DAPI, 4′,6-diamidino-2-phenylindole; FDR, false discovery rate; GO, gene ontology.

also been used to generate antimicrobial peptides. Despite the potential of machine-learning approaches, no computationally designed peptide has progressed beyond the early stages of experimental validation. Early computational design approaches were hindered due to the small number of antimicrobial peptides characterized and due to limitations in the algorithms used at the time. The rapid growth of antimicrobial peptide databases, and the maturation of language-based models, specifically LSTM networks, therefore provided the impetus for designing a new generation of synthetic antimicrobial peptides.

Here, antimicrobial peptide design has been cast as a computational language-modeling problem. Antimicrobial peptide sequences are treated as *words* of a 20-alphabet *language*. A long short-term memory (LSTM) model (30) is used to understand the arrangement and frequencies of amino acid residues within a peptide, which is analogous to the *grammar* of a language. Our model was used to generate, synthesize, and experimentally characterize 10 antimicrobial peptide sequences, of which one lead (NN2_0018) displayed promising *in vitro* and *in vivo* antimicrobial properties.

The primary focus of this work is on the characterization of NN2_0018 as a lead molecule. NN2_0018 inhibits ESBL, methicillin-resistant, and carbapenem-resistant clinical isolates *in vitro* and also demonstrated *in vivo* activity against carbapenem-resistant *Acinetobacter baumannii* in a mouse model of peritoneal infection. Furthermore, NN2_0018 displayed no mortality, hepatotoxicity, or nephrotoxicity at therapeutic doses. Circular dichroism, nuclear magnetic resonance (NMR), scanning electron microscopy, fluorescence microscopy, and microarray gene expression experiments shed light on the structure and mechanisms of action of NN2_0018. Secondarily, our results also show that the rational design of antimicrobial peptides is possible.

Results

Antimicrobial peptide design using LSTM language models

In this work, antimicrobial peptide design was cast as a language-modeling problem. As an analogy, antimicrobial peptides can be thought of as words in a language, created from 20 letters corresponding to 20 natural amino acid residues. The grammar of the language model is therefore the frequency and placement of amino acid residues. Given a sequence of amino acids x_1, x_2, …, x_{i-1}, … x_i, the language model attempts to predict the probability distribution over the amino acid vocabulary for the next amino acid in the sequence x_i. A probability distribution function of the form $P(x_i|x_{<i})$ is learned, where $x_{<i}$ refers to the sequence of residues before x_i (x_1 to x_{i-1}).

The LSTM model was trained on known antimicrobial sequences from the YADAMP (yet another database of antimicrobial peptides) database (9). As of September 2015, the YADAMP web server contained 2525 manually annotated sequences with their corresponding minimum inhibitory concentration (MIC) values. 1011 sequences (supporting Dataset S1, lstm.train) had a sequence length of ≤30 residues and were chosen as input for our LSTM algorithm. Sequences of >30 residues may form tertiary structures. Unlike a simple helical pattern, structural motifs that fold into complex patterns in three-dimensional (3D) space may not be properly captured by an algorithm optimized for deciphering sequential grammar. These sequences were therefore eliminated from our dataset. Our LSTM model generated 30,832 peptide sequences (supporting Dataset S1, lstm.sample). 17,390 sequences remained after removing sequences of >30 residues and redundant sequences using ClustalW (31).

Further filtering to select for positively charged amphiphilic peptides resulted in a dataset containing 6415 peptides (supporting Dataset S1, bilstm.out). For charge, we selected peptides possessing ≥4 positively charged residues (lysine, arginine, and histidine). For amphiphilicity, we used a simple index (H_*) to rapidly predict amphiphilicity for a large peptide sequence database. A peptide sequence was converted into a helical wheel projection on a two-dimensional (2D) polar coordinate plane (r, θ), with neighboring residues positioned 100° apart. Given a peptide sequence **S** composed of residues {r_1, r_2, … r_N}, we define $C_{\theta\ 204}$ **S** as the subset of residues that occur in the semicircle defined by θ in the anticlockwise direction. If $\mathbb{A}$ denotes the set of all polar residues, the score can be calculated using Equation 1.

$$H'_* = \max_{0 \le \theta \le 2\pi} \frac{\sum_{r_i \epsilon C_\theta} \delta_{r_i}}{\sum_{r_j \epsilon S} \delta_{r_j}}$$

$$H_* = (H'_* - 0.5) \times 2 \qquad \text{(Eq. 1)}$$

$$\delta_{r_i} = \begin{cases} 1, \text{ if } r_i \epsilon \mathbb{A} \\ 0, \text{ otherwise} \end{cases}$$

Note that 0.5 and 2 are scaling terms to re-scale the H'_* value from 0.5 → 1 to an H_* value of 0 → 1 (where 0 denotes no amphiphilicity and 1 denotes perfect amphiphilicity). Helices possessing H_* values of ≥0.33 (also containing ≥4 positively charged residues) were selected for further scoring using a Bi-LSTM (bi-directional long short-term memory) regression model.

A regression model was trained on 501 sequences (supporting Dataset S1, blstm.train) from the YADAMP database with available MIC data against *Escherichia coli*. It should be noted that our algorithm was not trained on toxicity data, as databases containing a sufficient quantity of toxicity data do not yet exist. MIC data were normalized to the range (0–1), where lower values correspond to lower MICs. To generate the vector representation of a sequence, a Bi-LSTM was used. The Bi-LSTM model utilizes two LSTMs (one that operates on the peptide sequence in the forward direction and one that operated on the sequence in reverse). Like the LSTM language model, the residues are fed one at a time. Our Bi-LSTM model ranked 6415 sequences based on their predicted antimicrobial activity (supporting Dataset S1, bilstm.out).

From these 6415 sequences, the best 10 sequences (NN2_0018 → NN2_0055 (1)) possessing the lowest Bi-LSTM scores were chosen for synthesis and experimental evaluation. These 10 sequences possessed Bi-LSTM scores ranging from 0.004135 → 0.010283. Three sequences (NN2_R0002, NN2_R0039, and NN2_R0048) possessing the poorest (highest) Bi-LSTM scores were also chosen for synthesis and experimentation, to act as

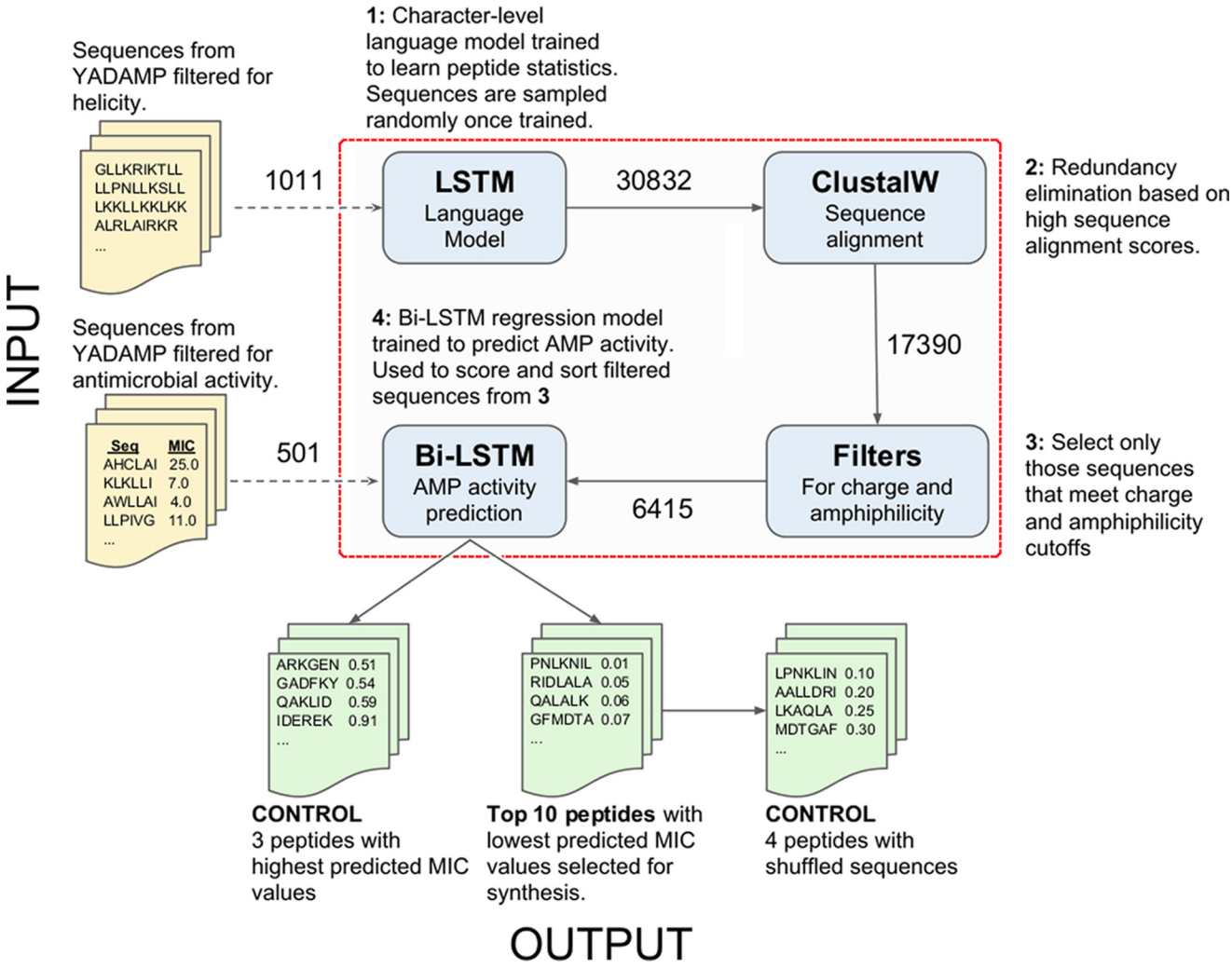

Figure 1. Workflow for the LSTM and Bi-LSTM algorithms, briefly describing the role of each step in the design of antimicrobial peptides. Steps involved in the algorithm itself are *boxed in red*. Inputs and outputs are excluded from this box.

negative controls. These three sequences possessed Bi-LSTM scores ranging from 0.551616 → 0.999483.

A workflow describing the algorithm's internal steps along with all inputs and outputs is provided in Fig. 1. An animation illustrating all the stages of this workflow is also provided (https://youtu.be/buMGrOprDsI).[3] Each of the stages is elaborated further in supporting Dataset S1, documentation.pdf. Our LSTM and Bi-LSTM algorithms are implemented in the Lua programming language relying on the Torch machine-learning library. The code for each of these stages and the entire pipeline have been uploaded to the GitHub repository (https://github.com/Tushar-N/amp-lm).[3]

Antimicrobial susceptibility testing of designed peptides

Using the residue-level LSTM language algorithm previously described, we synthesized and experimentally characterized 10 peptides possessing the lowest Bi-LSTM scores (Table 1). These peptides were assayed for antimicrobial activity using a broth microdilution method especially designed for cationic antimicrobial peptides (32), using peptide concentrations ranging from 0.25 → 128 μg/ml. 30 cultures were chosen for antimicrobial susceptibility testing based on their diversity and clinical relevance. Gram-positive, Gram-negative, fungal, and mycobacterial organisms were tested. Most cultures were acquired from the Microbial Type Culture Collection (MTCC, Chandigarh, India). Minimum inhibitory concentrations for all peptides and all cultures are provided in Table 2 (micromolar values are provided in Table S1). Designed peptides were scored based on the number of cultures they inhibited with the lowest MIC, as compared with the MICs of all other designed peptides (Equation 2).

$$\text{peptide\_score}_j = \sum_{i=1}^{M} \mathbb{I}\{X_{ij} = \min_{j=1}^{N}(X_i)\} \qquad \text{(Eq. 2)}$$

Here, X represents a matrix containing MIC values. M represents rows containing MIC values for a particular organism. N represents columns containing MIC values belonging to a particular peptide. Note that multiple minimum MIC values can occur along a given row. Using Equation 2, the two best

[3] Please note that the JBC is not responsible for the long-term archiving and maintenance of this site or any other third party hosted site.

Table 1

Names, sequences, solubilities, Bi-LSTM scores, peptide-positive charge, and amphiphilicity indices (*H) for all peptides synthesized and tested in this study are provided**

MIC values for all peptides against *E. coli* (K12 MG1655) are provided. For MIC values, *t* denotes test peptides, and *c* denotes control peptides. Test peptides possessed MIC values significantly lower than control peptides ($p = 0.029$, Welch Two-Sample *t* test).

Peptide	Sequence	solubility	Bi-LSTM score	positive charge	H_*	MIC_{ec} μg/mL (μM)
	Top-scoring peptides					
NN2_0018	YLARAIRRTLARLLL	≥10 mg/mL	0.004135	4	0.6	32^t (17.78)
NN2_0022	EWRVARRAVQRLRHLARRYH	≥20 mg/mL	0.004801	9	0.64	16^t (6.08)
NN2_0024	ALKKMLRLAKRLS	≥10 mg/mL	0.005227	5	0.67	64^t (41.89)
NN2_0027	VLSAFHKVIKIIHHISHF	2-10 mg/mL	0.005399	6	0.75	32^t (16.17)
NN2_0029	RKFRKILHRARKWI	≥20 mg/mL	0.005647	8	0.75	8^t (4.192)
NN2_0035	RRWGRWHRMRRRGR	≥20 mg/mL	0.006873	9	0.33	$>128^t$ (>63.29)
NN2_0039	FWKGLVKAAFKIVHAGS	2-10 mg/mL	0.007347	4	1.00	64^t (34.42)
NN2_0046	GWKAIHKAAKGIHTYVN	2-10 mg/mL	0.008279	5	1.00	$>128^t$ (>67.57)
NN2_0050	SWKKFFKKARSLPKLF	≥10 mg/mL	0.008996	6	0.75	4^t (2.00)
NN2_0055	YKRWKKWRSKAKKIL	≥10 mg/mL	0.010283	8	0.56	4^t (1.98)
	Worst-scoring peptides					
NN2_R0002	KWKCLAKVGIAAH	≥4 mg/mL	0.999483	4	0.5	128^c (89.84)
NN2_R0039	KRSWDIVKKYVGVVVGTIH	≥4 mg/mL	0.576789	5	0.5	128^c (58.59)
NN2_R0048	AGEKRIIKKIDEAFQ	≥4 mg/mL	0.551616	4	0.75	$>128^c$ (>73.31)
	Shuffled peptides					
NN2_0018_shuf1	AIARTRRRLLLYLLA	≥10 mg/mL	0.031060	4	0.6	$>128^c$ (>71.14)
NN2_0018_shuf2	AAARLRLLLYLITRR	≥10 mg/mL	0.036470	4	0.2	$>128^c$ (>71.14)
NN2_0050_shuf1	RKLAFKPLKKFFSWKS	≥10 mg/mL	0.117870	6	0.5	16^c (7.95)
NN2_0050_shuf2	SKFLSKKPKKLFWFRA	≥10 mg/mL	0.203130	6	0.25	$>128^c$ (>63.63)

performing peptides were identified as NN2_0050 and NN2_0018, with peptide scores of 15 and 10, respectively.

Two sets of control experiments were performed (Table 1). First, the MIC values of four peptides (NN2_0018_shuf1, NN2_0018_shuf2, NN2_0050_shuf1, and NN2_0050_shuf2) possessing shuffled sequences were obtained for *E. coli* (K12 MG1655). In all cases, the MIC values for unshuffled peptides were lower than their shuffled counterparts (Table 1), indicating that the grammar of NN2_0050 and NN2_0018 is critical for their efficacy. Second, we synthesized three peptides (NN2_R0002, NN2_R0039, and NN2_R0048) possessing high Bi-LSTM scores predicted to poorly inhibit *E. coli*. All three peptides displayed MIC values ≥128 μg/ml against *E. coli*, confirming that the Bi-LSTM algorithm could differentiate between effective and ineffective sequences. The MIC values of these seven control peptides were compared with those of NN2_0018 → NN2_0055. For *E. coli*, the control peptides displayed significantly higher MIC values ($p = 0.029$, Table 1). These results indicate that the Bi-LSTM algorithm was successfully trained using *E. coli* MIC values.

Antimicrobial susceptibility testing of our peptides against MDR clinical isolates

Antimicrobial susceptibility testing for NN2_0050 and NN2_0018 was performed against 61 recent clinical isolates obtained from MS Ramaiah Medical College, Bangalore, India (Table S2). Most isolates obtained displayed multidrug resistance (ESBL, methicillin resistance, and carbapenem resistance). Most isolates displayed mucoid morphologies not conducive to absorbance-based growth estimation. Therefore, minimum bactericidal concentration (MBC) for all cultures was assayed using the modified Resazurin protocol, as described under "Experimental procedures." NN2_0050 displayed greater activity against Gram-negative organisms. For NN2_0050, the Gram-negative MBC_{50} was found to be 4 μg/ml (2 μM), and the Gram-positive MBC_{50} was found to be 32 μg/ml (15.91 μM) (Table 3). NN2_0018 displayed slightly better activity against Gram-positive organisms. For NN2_0018, the Gram-negative MBC_{50} was found to be 16 μg/ml (8.88 μM), and the Gram-positive MBC_{50} was found to be 8 μg/ml (4.44 μM) (Table 4). However, NN2_0018 was found to possess greater activity against *Klebsiella pneumoniae* strains. Interestingly, NN2_0018 inhibited all 17 *Staphylococcus aureus* and CoNS strains tested with an MBC_{50} ≤16 μg/ml (8.88μM). All MRSA and methicillin-resistant CoNS isolates tested were also inhibited. A summary of all MBC values and conventional antibiotic resistance results for individual organisms is provided in Table S2.

In vitro and in vivo toxicity determination for designed peptides

Cytotoxicity experiments for NN2_0018 and NN2_0050 were performed on HeLa and HaCaT cells using the MTT assay. For HaCaT cells, both NN_0018 and NN2_0050 were found to possess negligible cytotoxicity (IC_{50} >128 μg/ml) in the concentration range tested (Fig. 2*A*). For HeLa cells, NN2_0018 displayed similar characteristics (IC_{50} >128 μg/ml). However, NN2_0050 possessed an IC_{50} <64 μg/ml (31.82 μM) (Fig. 2*B*). These results indicate that NN2_0050 lacks specificity for prokaryotic cells and may possess cross-reactivity against other eukaryotic tissues.

Based on the encouraging *in vitro* toxicity results obtained for NN2_0018, *in vivo* toxicity experiments were performed using 6–8-week-old BALB/c mice. Both female and male mice were used to account for gender differences in peptide toxicity.

Table 2

MIC values (in micrograms/ml) for all designed peptides against 30 cultures

MIC values in boldface type are the lowest MIC values for a given culture. Blank cells incidate that the MIC values exceed 128 μg/ml. Culture names marked with an asterisk indicate that the resazurin protocol was used to estimate MBC.

organism	culture ID	NN2_0018	NN2_0022	NN2_0024	NN2_0027	NN2_0029	NN2_0035	NN2_0039	NN2_0046	NN2_0050	NN2_0055
E. coli	K12 MG1655	32	16	64	32	8		64		**4**	**4**
A. baumannii	MTCC 9829	16	16	128	16	8		16		**4**	16
S. boydii	MTCC 11947	32	8	64	16	**1**	64			2	8
S. flexnerii	MTCC 1457	8	**1**	32	8	4	64			4	8
S. typhimurium	ATCC 14028	32	16			16				**8**	32
S. enterica	MTCC 9844	16	16	32	32	16				**8**	16
K. pneumoniae	MTCC 7407	**32**	128			64				**32**	128
K. oxytoca	MTCC 2275	16	**8**	128		32	64	64		16	32
P. aeruginosa	MTCC 3542		128			**16**				32	128
P. vulgaris	MTCC 1771	128	128			64				**16**	64
P. mirabilis	MTCC 3158										
C. koserii	MTCC 1657	16	16	64	16	64	16	64		**8**	16
C. freundii	MTCC 1658	**16**	64			32				32	128
N. mucosa *	MTCC 1772	**16**	32	128	32	32	64	128		**16**	64
V. cholerae	MTCC 3904	**64**	128			128			128	**64**	128
E. gergoviae	MTCC 3826	128	128							**64**	
H. influenzae	MTCC 621	8	8	64	8	8	128		64	**2**	32
A. faecalis	MTCC 1937	**32**	128			128				64	
B. bronchiseptica	MTCC 6837	4	2	8	4	**1**		8	128	**1**	8
E. aerogenes	MTCC 111	32								**16**	128
S. maltophilia	MTCC 1890	**16**	64			128		128		**16**	128
M. luteus *	MTCC 425	2	2	8	1	**0.25**	**0.25**	2	64	2	0.5
S. aureus	MTCC 3160	**16**				128				128	
S. haemolyticus	MTCC 3383	16	16	128	32	8	**4**	16		8	**4**
E. faecalis	MTCC 439	**64**								128	
C. glutamicum	MTCC 2679	4	**1**	16	4	2	4	2	64	2	2
C. pseudoTB *	MTCC 3158	**128**									
B. alcalophilis	MTCC 860	**16**	**16**		32	64	32	**16**		32	64
M. smegmatis *	MC2155	64	**16**	64	32	**16**	**16**	128		64	32
C. albicans *	MTCC 425	128	**64**	128		**64**	**64**			**64**	**64**
peptide score		10	6			7	4	1		15	3

NN2_0018 concentrations ranging from 32 → 256 μg/g (17.79 → 142.28 μmol/g) mouse body weight were tested. Six mice per cohort were used for each concentration, including a vehicle control (30 mice per gender). NN2_0018 suspended in buffer (20% DMSO, 80% saline) was injected intraperitoneally, and all mice were monitored for 7 days post-injection. All mice survived for 7 days post-injection at NN2_0018 concentrations up to 64 μg/g (35.57 μmol/g) (Fig. 2, *C* and *D*). Significant mortality was observed at 256 μg/g (142.28 μmol/g), with only 33% of female and male mice surviving for 7 days. Using linear interpolation, the LD_{50} of NN2_0018 was calculated to be 213 μg/g (118.38 μmol/g) for females and 224 μg/g (124.50 μmol/g) for males.

Blood tests were performed to determine whether NN2_0018 displays any hepatotoxic and nephrotoxic effects at 64 μg/g (35.57 μmol/g). These tests were performed on both female and male mice to account for gender differences in peptide toxicity. Four cohorts of six mice each (female-untreated, female-treated, male-untreated, and male-treated) were prepared.

Table 3
Distribution of MBCs of NN2_0050 for clinical isolates
MBC values tested range from 0.25 →128 μg/ml (0.12 →63.63 μM). This table is presented as a frequency distribution. Taking *S. aureus* as an example, NN2_0050 inhibited 1, 5, and 3 cultures with MBCs of 8, 32, and 64 μg/ml respectively.

organism	resistance	0.25 (0.12)	0.5 (0.25)	1 (0.5)	2 (1)	4 (2)	8 (4)	16 (7.95)	32 (15.91)	64 (31.81)	128 (63.63)	>128 (>63.63)	MBC_{50}
E. coli	CRE			1	2	2		2		2			
E. coli	ESBL			1	4	3		1					
E. coli						1							
total				2	6	6		3		2			4
A. baumannii	CRE				1	1		1					
A. baumannii					1								
total					2	1		1					2
K. pneumoniae	CRE					1	2			1	1		
K. pneumoniae	ESBL						1					2	
K. pneumoniae										1			
total						1	3			2	1	2	64
P. aeruginosa	CRE						1	1	2				
P. aeruginosa	ESBL						1						
P. aeruginosa					1	1							
total					1	1	2	1	2				8
E. faecalis									1	1		3	>128
CoNS	MRCN						3	1					
CoNS						1	2			1			
total						1	5	1		1			8
S. aureus	MRSA						1		1	1			
S. aureus									4	2			
total							1		5	3			32
Gram negative				2	9	9	5	5	2	4	1	2	4
Gram positive						1	6	1	6	5		3	32
total				2	9	10	11	6	8	9	1	5	8

Blood, liver, and kidney samples were extracted 24 h post-treatment. Blood urea nitrogen (kidneys, Fig. 2*E*) and aspartate aminotransferase (liver, Fig. 2*F*) concentrations for untreated *versus* treated cohorts displayed no significant differences, indicating that NN2_0018 does not possess acute hepatotoxic or nephrotoxic effects at 64 μg/g (35.57 μmol/g) for both female and male BALB/c mice.

Histopathological examination of liver and kidney sections stained with hematoxylin and eosin confirmed these findings. Liver sections displayed no necrosis or lipid vacuolation associated with liver damage (Fig. 3). Similarly, kidney sections from all four cohorts displayed no marked injuries. Renal tubules and glomeruli appeared intact. Characteristic cast formation, tubule dilation, or cytoplasmic vacuolation associated with drug-induced kidney damage was not detected (33, 34).

Survival experiments, blood tests, and histopathological tissue examination all indicate that NN2_0018 possesses no significant *in vivo* toxicity up to 64 μg/g (35.57 μmol/g), and therefore it has the potential for systemic use.

NN2_0018 clears carbapenem-resistant A. baumannii infections in vivo

NN2_0018 efficacy against *A. baumannii* (P1270) was assayed using the mouse peritoneal model of infection. Four cohorts of 6–8-week-old BALB/c mice (female) were infected through a peritoneal injection of 3.70×10^6 cfu of *A. baumannii* suspended in saline. Cohort 1 was euthanized at 0.5 h post-infection. A peritoneal cfu count was performed on this cohort to determine the pathogenic load at the start of treatment. Treatment began 0.5 h post-infection. Cohort 2 was treated with solvent (20% DMSO, 80% saline) to act as a sham control. Cohort 3 was treated with 13.33 μg/g (34.76 μmol/g) meropenem (a carbapenem-class drug) suspended in saline, corresponding to the Food and Drug Administration's (https://www.accessdata.fda.gov/drugsatfda_docs/label/2016/050706s037lbl.pdf) recommended dose for a 75-kg adult (35). Cohort 4 was treated with 64 μg/g (35.57 μmol/g) NN2_0018 in solvent (20% DMSO, 80% saline). Cohorts 2–4 were euthanized 4.5 h post-infection

Table 4
Distribution of MBCs of NN2_0018 for clinical isolates
MBC values tested range from 0.25 → 128 μg/ml (0.14 → 71.14 μM).

organism	resistance	0.25 (0.14)	0.5 (0.28)	1 (0.56)	2 (1.11)	4 (2.22)	8 (4.45)	16 (8.89)	32 (17.79)	64 (35.57)	128 (71.14)	>128 (>71.14)	MBC_{50}
E. coli	CRE					2	3	1	1	1	1		
E. coli	ESBL				1	4	3			1			
E. coli							1						
total					1	6	7	1	1	2	1		8
A. baumannii	CRE						2			1			
A. baumannii								1					
total							2	1		1			8
K. pneumoniae	CRE						2	1		1	1		
K. pneumoniae	ESBL						1	1		1			
K. pneumoniae									1				
total							3	2	1	2	1		16
P. aeruginosa	CRE									1	1	2	
P. aeruginosa	ESBL									1			
P. aeruginosa										2			
total										4	1	2	64
E. faecalis							1	1	1	2			32
CoNS	MRCN					1	2	1					
CoNS						2	2						
total						3	4	1					8
S.aureus	MRSA						2	1					
S.aureus							1	5					
total							3	6					16
Gram negative					1	6	12	4	2	9	3	2	16
Gram positive						3	8	8	1	2			8
total					1	9	20	12	3	11	3	2	16

(4 h post-treatment), and peritoneal cfu counts were performed for all mice. This experimental setup is illustrated in Fig. 4*A*. Statistical analyses were performed using a one-way ANOVA. Globally, the one-way ANOVA displayed a p value 5.83×10^{-6}, indicating that there were statistically significant differences between the means of these cohorts. To determine which cohorts possessed significantly different means, further statistical testing was performed using the pairwise Tukey's HSD (honest significant difference) tests. Pairwise Tukey's HSD tests possessing $p < 0.05$ are reported.

A. baumannii (P1270) displayed rapid, exponential growth in mice (Fig. 4*B*). The initial peritoneal inoculum of 3.70×10^6 cfu increased to 5.52×10^6 cfu at 0.5 h in Cohort 1, indicating a doubling time of 51 min (0 → 0.5-h interval). Furthermore, the peritoneal load increased to 2.11×10^8 cfu at 4.5 h post-infection in Cohort 2, indicating a similar doubling time of 45 min (0.5 → 4.5-h interval).

From a pre-treatment (0.5 h) load of 5.52×10^6 in Cohort 1, the peritoneal load increased to 2.11×10^8 cfu at 4.5 h post-infection in Cohort 2 (sham-treated, $p = 0.0005$) and 1.98×10^8 cfu in Cohort 3 (meropenem-treated, $p = 0.0002$) (Fig. 4*B*). These results indicate that both sham and meropenem treatment are ineffective at reducing peritoneal cfu loads of *A. baumannii* (P1270).

In contrast, NN2_0018 was found to significantly lower peritoneal *A. baumannii* (P1270) loads for Cohort 4 (Fig. 4*B*), in comparison with both sham-treated Cohort 2 ($p = 0.0002$) and meropenem-treated Cohort 3 ($p = 0.0001$). The mean peritoneal cfu load for NN2_0018-treated Cohort 4 was 3.53×10^6, in comparison with the sham-treated and meropenem-treated peritoneal cfu loads of 2.11×10^8 and 1.98×10^8 cfu, respectively. These results indicate that NN2_0018 is more effective at reducing carbapenem-resistant *A. baumannii* loads *in vivo* than both sham and meropenem treatment.

SEM visualization of peptide-induced membrane disruption

Membrane disruptions were studied using scanning electron microscopy experiments. We chose *E. coli* (K12 MG1655) and *Staphylococcus hemolyticus* (MTCC 3383) as model Gram-negative and Gram-positive organisms, respectively. NN2_0050 and NN2_0018 were chosen for these experiments. Fig. 5, *A–C,*

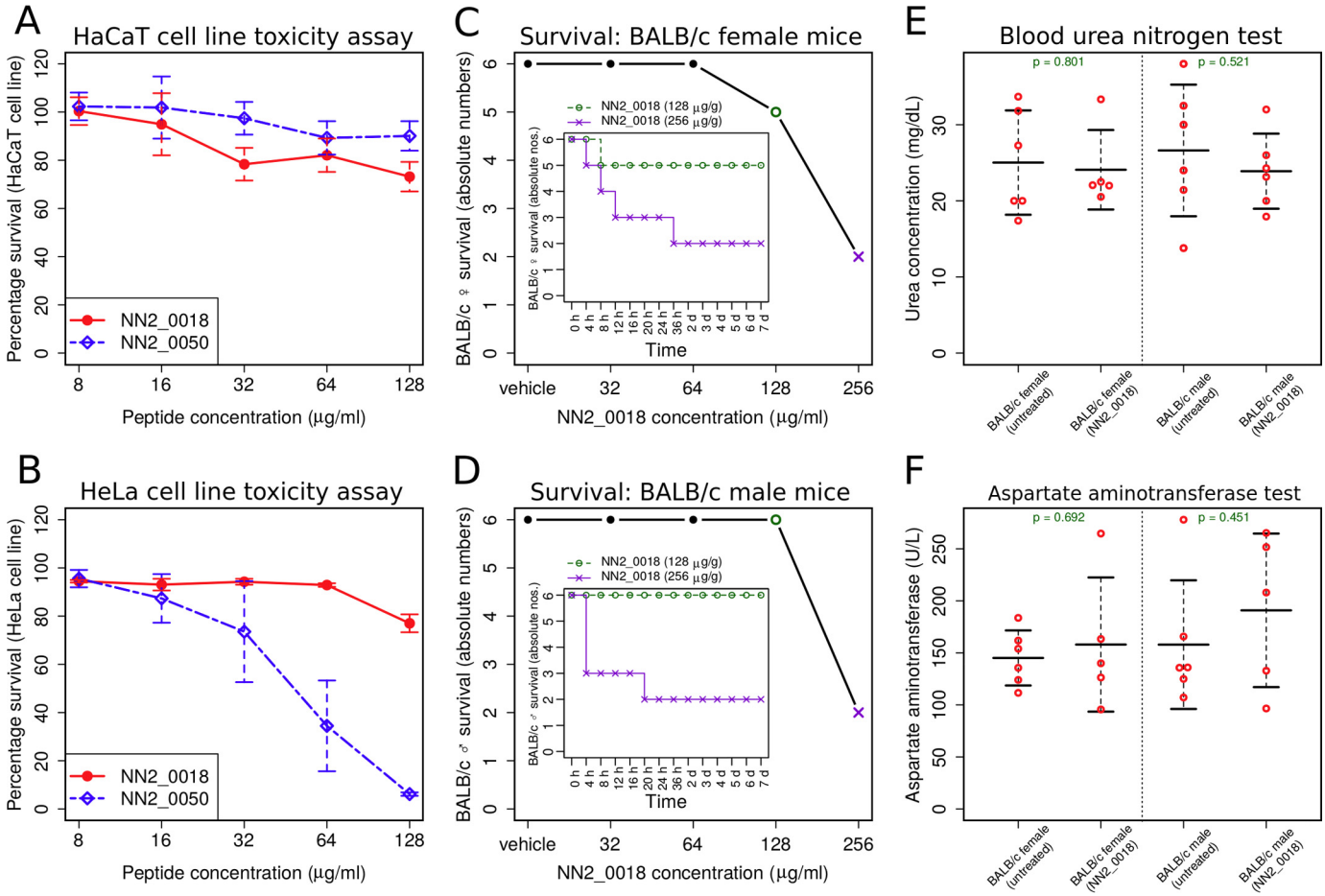

Figure 2. *In vitro* and *in vivo* toxicity assays. *A, in vitro* cytotoxicity assay for peptides NN2_0018 and NN2_0050 using the HeLa cell line. *B, in vitro* cytotoxicity assay for peptides NN2_0018 and NN2_0050 using the HaCaT cell line. *C, in vivo* systemic toxicity assay for NN2_0018 using a BALB/c mouse model (female). *Inset*, Kaplan-Meier plot for mouse survival (BALB/c, female) at 128 μg/g (71.14 μmol/g) and 256 μg/g (142.28 μmol/g) NN2_0018. *D, in vivo* systemic toxicity assay for NN2_0018 using a BALB/c mouse model (male). *Inset,* Kaplan-Meier plot for mouse survival (BALB/c, male) at 128 μg/g (71.14 μmol/g) and 256 μg/g (142.28 μmol/g) NN2_0018. Note that six mice were used for each NN2_0018 concentration tested (including a buffer-only vehicle control). *E* and *F*, blood tests performed for both male and female BALB/c mice to determine toxicity at therapeutic NN2_0018 doses. In all cases, treated cohorts were injected with 64 μg/g (35.57 μmol/g) NN2_0018 in buffer and incubated for 24 h before blood extraction. *p* values (in *green*) were calculated using the Welch two-sample *t* test. *E,* blood urea nitrogen assay. *F,* aspartate aminotransferase assay. For all cases, peptide concentration units are expressed as micrograms of g peptide per g of mouse body weight (or micromoles of peptide per g of mouse body weight).

depicts the effect of NN2_0050 and NN2_0018 on *E. coli* cellular morphology.

In the absence of the antimicrobial peptides, *E. coli* cells display typical morphological characteristics, remaining turgid, smooth, and cylindrically shaped (Fig. 5*A*). The addition of NN2_0018 dramatically alters *E. coli* cellular morphology. *E. coli* cells appeared highly ridged and flattened (Fig. 5*B*), implying a substantial loss of cytoplasmic contents through membrane rupture.

The addition of NN2_0050 produced similar morphological changes. *E. coli* cells appeared flaccid and highly ridged along most of their surface (Fig. 5*C*). Direct evidence of membrane rupture was observed. The leakage of cellular contents from lysed cells can be observed in the *top-left region* of Fig. 5*C*.

Although *S. hemolyticus* was observed to be susceptible to NN2_0050 and NN2_0018, it displayed little morphological change upon peptide addition. Untreated *S. hemolyticus* cells display typical morphological characteristics, remaining turgid, smooth, and spherical (Fig. 5*D*). The addition of NN2_0018 produced no morphological changes (Fig. 5*E*). Similarly, the addition of NN2_0050 brought about no morphological changes (Fig. 5*F*). Low magnification (×10,000) SEM images for all samples are provided in Fig. S1, *A–F*.

We hypothesized that the thicker, peptidoglycan-rich Gram-positive cell wall prevented the observation of large-scale morphological disruptions for *S. hemolyticus*. Therefore, we removed the cell wall via induced protoplast formation using benzylpenicillin (36). Protoplast formation was confirmed through Gram staining (Fig. S2, *A* and *B*). Untreated *S. hemolyticus* protoplasts retained a smooth, spherical shape despite completely lacking a cell wall (Fig. 5*G*). *S. hemolyticus* protoplasts treated with NN2_0018 displayed membrane perforations and minor blebbing (Fig. 5*H*). Protoplasts treated with NN2_0050 displayed similar perforations and more prominent cell-membrane blebbing (Fig. 5*I*). Low magnification (×20,000) SEM images for all *S. hemolyticus* protoplasts are provided Fig. S3, *A–C*. These observations confirm that both Gram-positive and Gram-negative cells are susceptible to membrane disruption induced by peptides NN2_0018 and NN2_0050.

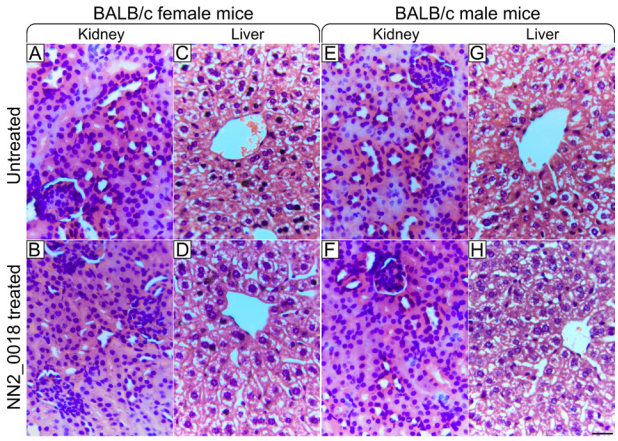

Figure 3. Histopathological examination of BALB/c mouse liver and kidney sections. *A,* representative kidney section from an untreated female mouse. *B,* representative kidney section from an NN2_0018-treated female mouse. *C,* representative liver section from an untreated female mouse. *D,* representative liver section from an NN2_0018-treated female mouse. *E,* representative kidney section from an untreated male mouse. *F,* representative kidney section from an NN2_0018-treated male mouse. *G,* representative liver section from an untreated male mouse. *H,* representative liver section from an NN2_0018-treated male mouse. All treated mice were injected with 64 μg/g (35.57 μmol/g) NN2_0018 in buffer (20% DMSO, 80% saline) and incubated for 24 h before euthanization through a ketamine overdose. All sections were stained using hematoxylin and eosin. All images were visualized using a ×40 objective. The *scale bar* (*black, bottom right*) represents 20 μm.

Peptide localization within bacterial cell membranes

Peptide localization experiments were performed by observing FITC-labeled peptides using confocal microscopy. *E. coli* (K12 MG1655) and *S. hemolyticus* (MTCC 3383) were incubated with FITC-labeled NN2_0018 and NN2_0050 and counterstained with DAPI (nucleic acid staining) and Nile red (lipid/cell membrane staining). All images were acquired using a ×63 oil immersion lens. For clarity, a representative region for all images was chosen and further magnified digitally at ×3. All original images can be found in supporting Dataset S2.

NN2_0018 was observed to colocalize with Nile red (Fig. 6*A*), confirming peptide localization in the cell membrane. Both *E. coli* and *S. hemolyticus* display similar colocalization characteristics. NN2_0050 was also observed to localize predominantly within the cell membrane for both *E. coli* and *S. hemolyticus* (Fig. 6*B*).

Confocal microscopy confirmed that NN2_0050 causes large-scale *S. hemolyticus* cell membrane disruption. In Fig. 6*B* (Nile red/FITC-peptide), *S. hemolyticus* cell membranes appeared shrunken and distorted, in contrast to the large, spherical membranes visualized in Fig. 6*A* (Nile red/FITC-peptide). SEM experiments revealed that NN2_0050 was able to penetrate the peptidoglycan layer without causing any disruptions. Both experimental approaches therefore indicate that NN2_0050 ultimately localizes in the cell membrane, causing large-scale disruptions. These disruptions remained contained within the unperturbed peptidoglycan-rich cell wall.

Pearson's correlation was used to quantify colocalization for all combined images in Fig. 6. Initially, K-means clustering was performed, partitioning image pixels into two clusters (cell and background). For the cell body, pixel-pixel intensity correlations for all combinations of stain channels was calculated using Pearson's correlation. Higher correlation values represented better stain colocalization. In all cases, Nile red/FITC-peptide displayed the highest correlation, confirming that our designed peptides colocalize within membranes (Fig. 6*C*).

Differential E. coli gene expression upon NN2_0018 challenge

Two replicates of a carbapenem-resistant *E. coli* clinical isolate (P1645ec) were challenged with NN2_0018 at half-MBC concentrations (4 μg/ml, 2.22 μM). Two control replicates grown under identical conditions but lacking NN2_0018 challenge were also prepared. RNA expression levels of all four samples were compared using an Agilent comparative genomic hybridization (CGH) microarray platform. Differentially expressed genes (DEGs) showing at least 1.319 ($2^{0.4}$)-fold up-regulation or down-regulation were identified between NN2_0018-challenged and unchallenged samples. A ClueGO comprehensive enrichment analysis was performed on these DEGs to classify genes into functional groups. Our ClueGO classification resulted in a total of 74 up-regulated and 15 down-regulated genes, classified into 15 functional groups (Fig. 7*A* and Table S3) and seven functional groups (Fig. 7*B* and Table S4), respectively. Genes from these functional groups were then individually annotated based on a literature survey (Table 5).

42 of 74 up-regulated genes belong to stress-response proteins, indicating that nonspecific stress response plays a major role in the pathogen's response to NN2_0018 challenge. These genes were associated with DNA repair (14), heat stress (8), reactive oxygen species stress (5), acid stress (6), osmotic stress (4), cation homeostasis (3), biofilm formation (4), carbonyl stress (1), protein repair (1), and other stress responses (3). Note that some genes are associated with multiple stress responses.

Three genes associated with virulence factors were up-regulated: *phoB*, *cyaA*, and *ihfB*. *phoB*, part of the phosphate regulon, is required for virulence expression across multiple organisms (37). *cyaA* (bifunctional hemolysin/adenylate cyclase) is responsible for respiratory tract colonization (38–40). *ihfB* (integration host factor) is also known to regulate virulence gene expression across multiple organisms (41, 42). Pathogens up-regulate virulence factor gene expression in response to stress (37), and these genes can therefore be considered as part of the nonspecific stress response.

Two genes associated with cell membrane integrity were up-regulated. *ompR*, a transcriptional regulator of major outer membrane protein genes, was up-regulated. Outer membrane proteins maintain lipid asymmetry in the outer membrane, serving both a structural role and preventing cellular entry of toxins (43). *cfa* (cyclopropane–fatty-acyl–phospholipid synthase) was also up-regulated. Cyclopropane fatty acids are known to stabilize membranes by decreasing mobility and increasing lipid bilayer packing tightness (44–47). These results indicate that *ompR* and *cfa* may be up-regulated to compensate for NN2_0018-induced membrane disruption.

Five genes associated with electron transport were up-regulated: *erpA* (essential respiratory protein), *frdB*, *frdC*, and *frdD* (fumarate reductase complex), and *cydA* (cytochrome *bd*-I ubiquinol oxidase subunit 1). *erpA* remains essential in the presence of oxygen or alternative electron acceptors (48). *cydA* is a terminal oxidase that predominates under low aeration

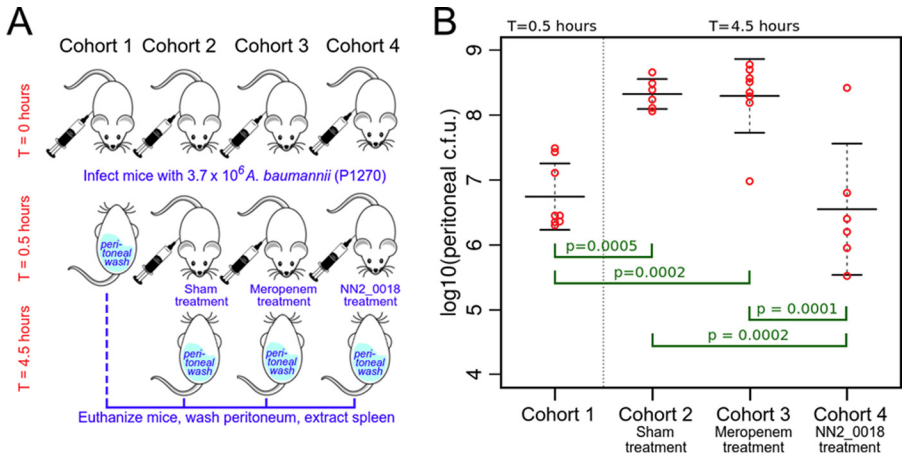

Figure 4. *In vivo* efficacy of NN2_0018 against carbapenem-resistant *A. baumannii* (P1270). *A,* experimental setup for *in vivo* efficacy determination using BALB/c mice (female, 6–8 weeks old). *B,* peritoneal cfu count for cohorts 1–4. Peritoneal cfu loads for the NN2_0018-treated cohort are significantly lower than for the sham-treated or meropenem-treated cohorts. Cohort 3 was treated with 13.33 μg/g (34.76 μmol/g) meropenem. Cohort 4 was treated with 64 μg/g (35.57 μmol/g) NN2_0018. *Error bars* indicate mean and standard deviation. All *p* values were calculated using the pairwise Tukey's honest significant difference (HSD) test.

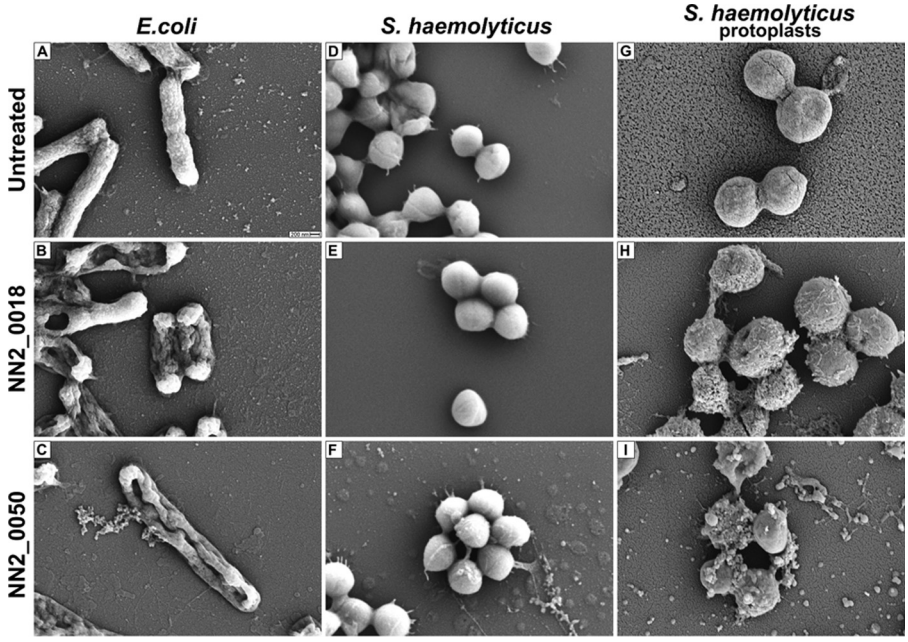

Figure 5. Scanning electron microscopy experiments performed on *E. coli* (K12 MG1655), *S. hemolyticus* (MTCC 3383), and *S. hemolyticus* protoplasts. *A,* untreated *E. coli* cells observed under ×50,000 magnification. *B, E. coli* cells treated with NN2_0018. Membrane disruption is visible. *C, E. coli* cells treated with NN2_0050. Membrane disruption and exudation of cytoplasmic contents is apparent. *D,* untreated *S. hemolyticus* cells observed under ×50,000 magnification. *E, S. hemolyticus* cells treated with NN2_0018. *F, S. hemolyticus* cells treated with NN2_0050, displaying some exudation of cytoplasmic contents. *G,* untreated *S. hemolyticus* protoplasts observed under ×50,000 magnification. *H, S. hemolyticus* protoplasts treated with NN2_0018 observed under ×50,000 magnification. Membrane perforations and leakage of cytoplasmic contents is easily observable. *I, S. hemolyticus* protoplasts treated with NN2_0050 observed under ×50,000 magnification. Blebbing is easily observable on all cell membranes. Detached blebs are also observable around protoplasts as *small spheres*. *B, E,* and *H,* 128 μg/ml (71.14 μM) of NN2_0018 was used. *C, F,* and *I,* 128 μg/ml (63.63 μM) of NN2_0050 was used.

(49). Fumarate reductase acts as a terminal electron acceptor during anaerobic respiration only, accepting electrons from complex I via naphthoquinones (50). The up-regulation of anaerobic electron transport components implies that oxygen uptake by, or electron transport to, cytochrome *c* oxidase has been inhibited. It is conceivable that NN2_0018 inhibits electron transport chain complexes II → IV (cytochrome *c* oxidase) or terminal oxygen uptake, forcing the up-regulation of anaerobic electron transport chain components.

Ten genes associated with carbohydrate degradation were up-regulated. These genes were associated with glycolysis (*deoC*, *dmlA*, *gapA*, and *yeaD*), the pentose phosphate pathway (*pgl* and *tktB*), glycogen metabolism (*glgP* and *glgS*), galactose metabolism (*galT*), and trehalose metabolism (*otsB*). The up-regulation of these genes may be a response to increasing cellular energy demands, potentially due to the energetic demands of stress responses and to compensate for decreased oxidative electron transport.

Four genes (*thiC*, *thiD*, *thiE*, and *thiG*) associated with thiamine production were down-regulated. Four ABC transporter genes, *fepD* (iron transport), *glnH* (glutamine-transport), *lolC* (lipoprotein transport), and *malE* (maltose transport), were

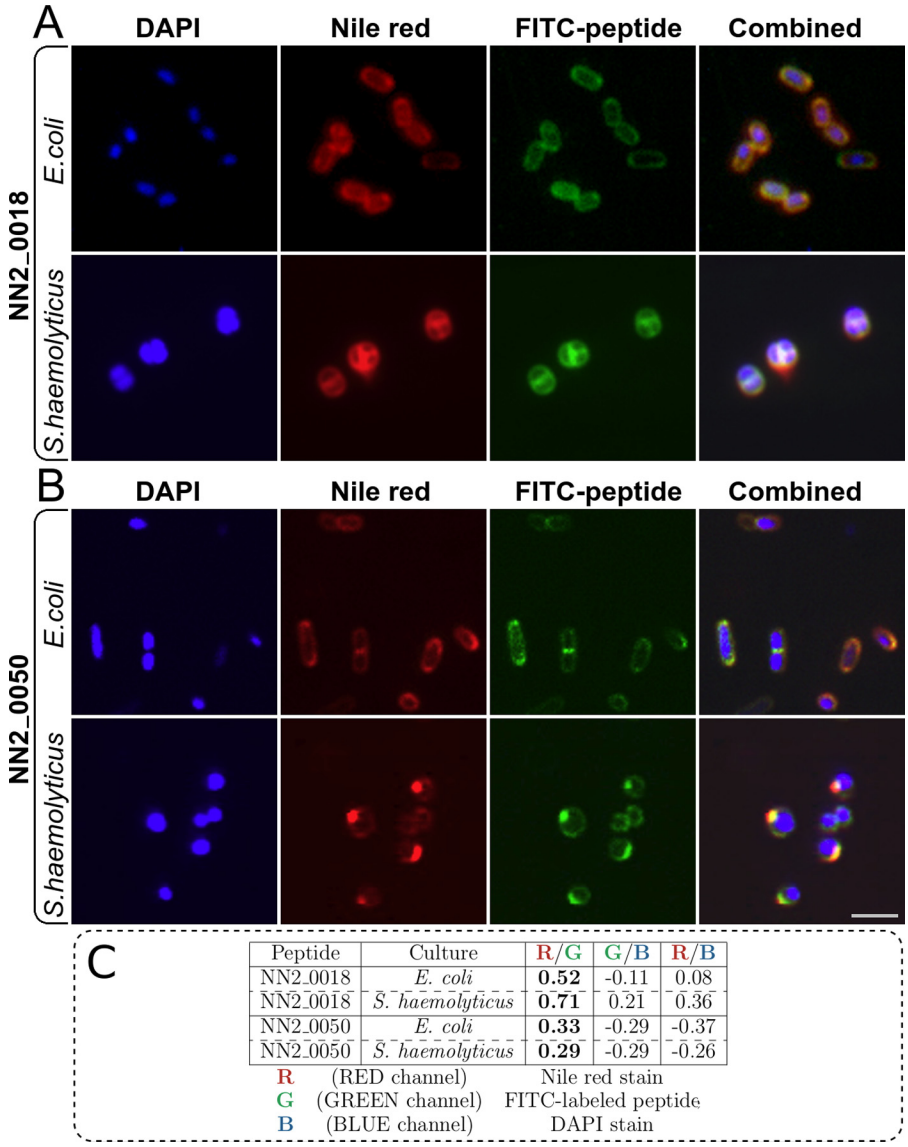

Peptide	Culture	R/G	G/B	R/B
NN2_0018	*E. coli*	**0.52**	-0.11	0.08
NN2_0018	*S. haemolyticus*	**0.71**	0.21	0.36
NN2_0050	*E. coli*	**0.33**	-0.29	-0.37
NN2_0050	*S. haemolyticus*	**0.29**	-0.29	-0.26

Figure 6. Confocal microscopy experiments performed on *E. coli* (K12 MG1655) and *S. hemolyticus* (MTCC 3383) cells, using FITC-labeled peptides NN2_0018 and NN2_0050. *A, E. coli* and *S. hemolyticus* treated with FITC-labeled NN2_0018. In both cases, NN2_0018 was found to colocalize with Nile red, indicating a strong membrane-binding preference. *B, E. coli* and *S. hemolyticus* treated with FITC-labeled NN2_0050. Again, NN2_0050 was found to colocalize with Nile red, indicating a membrane-binding preference. Here, membrane destabilization is apparent for *S. hemolyticus*. 8 μg/ml (4.44 μM) NN2_0018 and 8 μg/ml (4 μM) NN2_0050 were used. All images have been captured using a ×63 oil immersion objective. For clarity, all images have been digitally magnified by an additional ×3. The *scale bar* (*gray, bottom right*) represents 2 μm. *C,* Pearson's correlation coefficients for all stain combinations (DAPI/FITC-peptide/Nile red). Higher correlations denote better stain colocalization. In all cases, Nile red/FITC-peptide stains showed the highest correlation values.

also down-regulated. The reasons for the differential expression of these eight genes, along with 19 other DEGs, are not apparent and merit further investigation. All DEGs and pathway alterations constituting the *E. coli* response to NN2_0018 challenge are depicted in Fig. 8.

Preliminary structural characterization of NN2_0018

Circular dichroism experiments revealed that NN2_0018 adopts a random-coil configuration in water, indicating that NN2_0018 remains disordered outside the cellular environment. However, spectra displaying α-helical characteristics (minima at 222 nm and 208 nm) were recorded in apolar solvents such as methanol, 15 mM dodecylphosphocholine (DPC) micelles, and 40% trifluoroethanol (Fig. 9*A*), indicating that NN2_0018 adopts an α-helical conformation upon interacting with environments mimicking the bacterial cell membrane. The 1D NMR spectrum of NN2_0018 in both deuterated DPC micelles and deuterated methanol possessed well resolved chemical shifts in the amide region (Fig. 9*B*), indicative of a well-folded peptide. The vast majority of α-protons in NN2_0018 resonate at chemical shifts below 4.5 ppm, indicating that the peptide adopts an α-helical conformation in both solvents. The NOESY NMR spectrum of NN2_0018 possessed several cross-peaks in the amide (7–9 ppm) region for both deuterated methanol (Fig. 9*C*) and DPC micelles (Fig. 9*D*). These cross-peaks indicate the spatial proximity of amide protons of adjacent residues ($i \rightarrow i + 1, i \rightarrow i + 2$), characteristic of α-helices, confirming that NN2_0018 adopts an α-helical structure in apolar environments. The cross-peaks are more numerous and possess greater intensities in DPC micelles, indi-

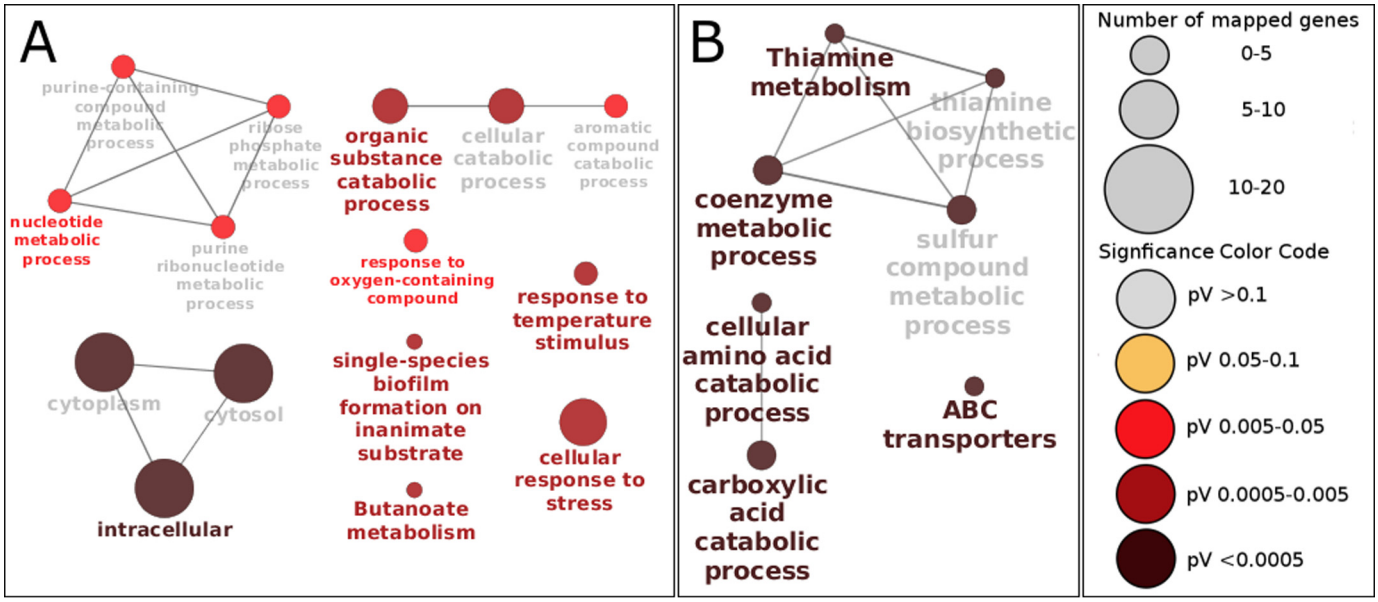

Figure 7. Functional groups derived from a ClueGO enrichment analysis. *A,* 15 functional groups were identified for up-regulated genes. *B,* seven functional groups were identified for down-regulated genes. Node color corresponds to the significance of the functional groups enriched (*brown* <0.0005 and *gray* >0.1). Node size corresponds to the number of mapped genes for a particular functional group. Edges represent shared genes between two functional groups. Edge thickness is proportional to the number of shared genes. Nodes containing genes that are subsets of other nodes have labels colored *gray*.

Table 5

DEGs for carbapenem-resistant *E. coli* (P1645ec) upon challenge with NN2_0018 (4 μg/ml or 2.22 μM, half-MBC)

Function	Associated genes (UPREGULATED)
DNA damage	aidB, nfi, purC, purD, purL, deoD, yceK, ycfH, ycgB, yciE, yciF, ydiZ, yggE, sbmC
Heat stress	clpB, cspC, grpE, hchA, hslU, hslV, ttdB, yggE
ROS stress	ariR, grxB, katE, yggE, ygiW
Acid stress	gadA, gadW, glsA, hchA, hdeA, hdeB
Osmotic stress	manX, manY, nhaA, grpE
Cation homeostasis	cueR, yegE, ynfG
Biofilm formation	ariR, dctR, ychH, ygiW
Carbonyl stress	hchA
Protein repair	pcm
Other stress	cbpA, grcA, rcsB
Virulence factors	phoB, cyaA, ihfB
Cell-membrane integrity	ompR, cfa
Electron transport	cydA, erpA, frdB, frdC, frdD
Carbohydrate degradation	deoC, dmlA, gapA, yeaD, pgl, tktB, glgP, glgS, galT, otsB
Other upregulated	tnaB, elaB, mioC, msyB, nadD, phnP, ydcY, yfcZ, ygdH, speA, patD, rne
	Associated genes (DOWNREGULATED)
Thiamine synthesis	thiC, thiD, thiE, thiG
ABC transporters	fepD, glnH, lolC, malE
Other downregulated	acnB, acs, astC, dadA, rspA, sucB, uidA

cating that NN2_0018 displays greater helical structure in DPC. Further structural characterization of NN2_0018 is in progress.

Discussion

The emergence of MDR pathogens poses a grave public health problem. Of particular concern is the emergence of carbapenem-resistant pathogens, as such pathogens are difficult to treat and result in poor clinical outcomes. There is therefore an urgent need for new antimicrobial compounds to address proliferating drug resistance. In this work, we have implemented an LSTM model to understand and design antimicrobial peptides. Our model correctly understood the underlying grammar of antimicrobial peptide sequences, as demonstrated by the broad-spectrum antimicrobial activity of all our designed peptides. Our two best peptide designs (NN2_0050 and NN2_0018) were found to display activity against MDR clinical isolates, including carbapenem-resistant and methicillin-resistant organisms.

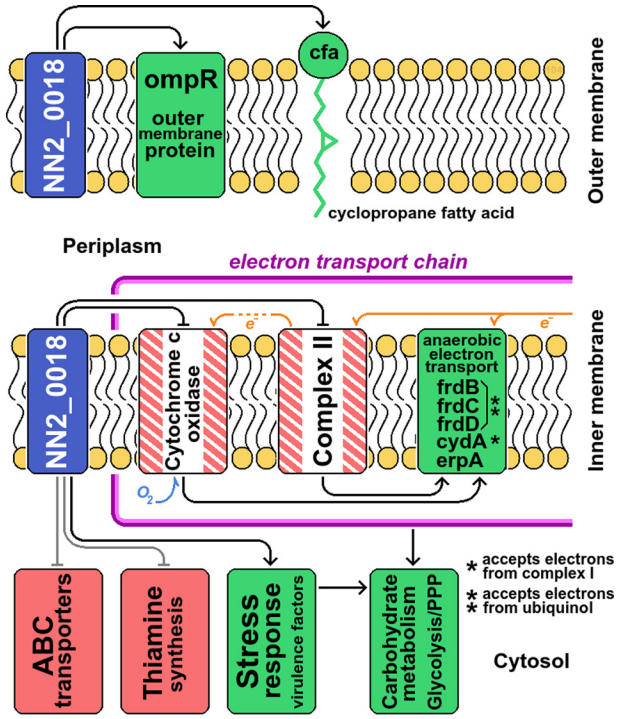

Figure 8. Molecular response of *E. coli* (P1645ec) to NN2_0018 challenge is shown. Up-regulated and down-regulated genes observed directly from microarray data are colored *green* and *red*, respectively. NN2_0018 targets inferred but not directly observed from microarray data are shaded as *red lines*. For clarity, most individual DEGs are not shown in favor of depicting pathways/functions. Genes associated with each pathway/function can be found in Table 5. DEGs whose down-regulation could not be rationalized are depicted with *gray edges*.

Toxicity has hindered past efforts aimed at developing systemic therapeutic peptides. For example, gramicidin S and melittin (51) possess high hemolytic activities. Encouragingly, NN2_0018 displayed minimal toxicity at bactericidal

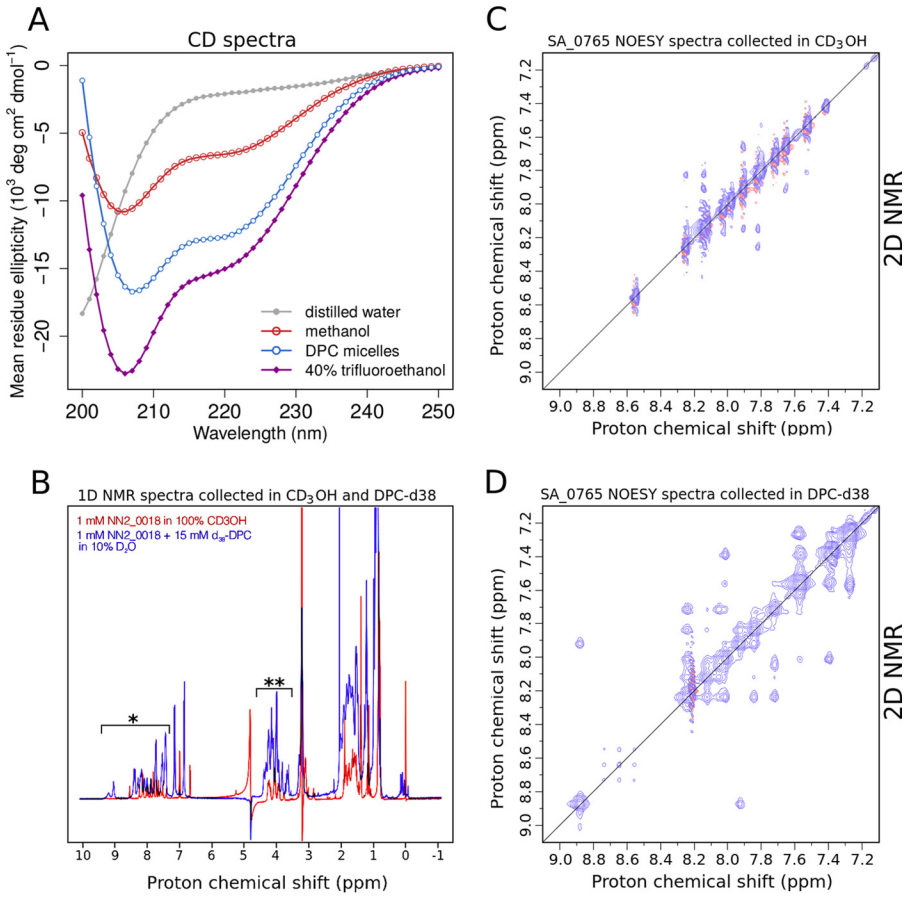

Figure 9. Structural characterization of NN2_0018. *A,* near-UV CD spectra of NN2_0018 displaying a random coil configuration in distilled water. NN2_0018 adopts an α-helical conformation in apolar solvents (methanol, 15 mM dodecylphosphocholine micelles, and 40% trifluoroethanol). *B,* 1D NMR spectrum of NN2_0018 acquired in deuterated dodecylphosphocholine micelles (*blue*) and deuterated methanol (*red*). *, well-resolved chemical shift dispersion in the amide region indicates proper folding. **, α-protons appear below 4.5 ppm as well resolved peaks, indicating α-helical structure. Chemical shift dispersion was more pronounced in dodecylphosphocholine micelles, indicating greater helical content. *C,* NOESY NMR spectrum of NN2_0018 acquired in deuterated methanol. *D,* NOESY NMR spectrum of NN2_0018 acquired in 15 mM deuterated dodecylphosphocholine micelles. Cross-peaks in the amide (7–9 ppm) region are indicative of α-helical structures. Positive contours are colored *blue*, and negative contours are colored *orange*. In all cases, 1 mM NN2_0018 was used.

concentrations when tested *in vitro* against the HaCat and HeLa cell lines and *in vivo* against BALB/c mice. Furthermore, NN2_0018 displayed *in vivo* efficacy against carbapenem-resistant *A. baumannii*. Our selection of carbapenem-resistant *A. baumannii* for *in vivo* texting was motivated by its Priority-1 classification (52) as a critical pathogen for the development of new drugs. Because of both efficacy against MDR clinical isolates and low *in vivo* toxicity, the algorithms and peptides described in this work represent a significant advancement over previous language models (28). Such models produced peptides that failed to display sufficient efficacy (only 4/40 peptides possessed MICs $\leq$64 μg/ml against *E. coli*).

We further investigated the mechanisms of action of our best designs, and we concluded that their antimicrobial activity is primarily due to direct membrane interaction and disruption, with secondary systemic effects. Peptide localization into membranes was observed using confocal microscopy. Peptide-induced membrane disruptions involving prominent blebbing and exudation of cellular contents were observed using SEM. Microarray gene expression analysis revealed that *E. coli* responds to NN2_0018 challenge through stress responses as well as pathway-specific responses. Anaerobic electron transport proteins were found to be up-regulated, implying that NN2_0018 hinders oxidative electron transport. Different antimicrobial peptides have been shown to elicit unique bacterial gene expression responses (53), therefore implying that the responses characterized in this study may be specific to NN2_0018 challenge.

NN2_0018 appeared α-helical and well-folded in a micellar environment. Structural elucidation and structure-function analyses are important future steps in the characterization of NN2_0018. In particular, the mechanisms responsible for the differential activity of NN2_0018 and NN2_0050 for Gram-negative and Gram-positive organisms deserve further investigation. The mechanism of action of antimicrobial peptides does not depend on a specific molecular target. Instead, an entire cellular component (the cell membrane) is disrupted, which makes the development of resistance against them difficult. Ultimately, our experimentally validated LSTM algorithms and peptides may help design new peptide-based antibiotics. Such antibiotics are needed to counter the ever-increasing problem of multiple drug resistance.

Experimental procedures

Peptide synthesis

All peptides synthesized for this study were procured from Genscript, Inc. 20 mg of all 17 NN2 (10), NN2_shuf* (4), and NN2_R* (3) family peptides were synthesized as part of a peptide library. Peptides NN2_0018 (93.3% purity) and NN2_0050 (93.0% purity) were individually synthesized for further characterization. Peptide synthesis of FITC-labeled NN2_0018 (92.7% purity) and NN2_0050 (87.1% purity) was performed individually. High-purity NN2_0050 (95.4% purity) was synthesized for *in vivo* toxicity and efficacy experiments. HPLC and liquid chromatography-mass spectrometry experiments confirmed the molecular weights and purity of these peptides (supporting Dataset S3).

Antimicrobial susceptibility assays

The MIC of a given peptide and for a given organism was determined using the microwell dilution method, as described by Wiegand *et al.* (32) (Protocol E). This protocol was optimized for determining the MIC of cationic antimicrobial peptides. Briefly, the protocol is as follows: 2-fold dilutions of the peptide were created in a sterile 96-well polypropylene plate. Ten peptide concentrations were used, ranging from 256 → 0.5 μg/ml. Each well contained the peptide diluted in Mueller Hinton (MH) broth (Sigma: 70192-100G), as well as the culture being assayed. At this stage, each well contained 50 μl of peptide in Mueller Hinton broth.

Cultures to be assayed were grown in Mueller Hinton broth and incubated overnight at 37 °C under shaker conditions of 180 rpm. The culture was diluted to 10^8 cfu/ml by comparing the absorbance at 600 nm with that of the MacFarland 0.5 standard. A further 1:100 dilution was performed using Mueller Hinton broth, reducing the number of colony-forming units to 10^6 cfu/ml. Spread plating was used to confirm the expected colony count. Each of the 10 wells described previously was inoculated with 50 μl of this culture, resulting in a final inoculum of 5×10^5 or 5×10^4 cfu/well. Note that the addition of 50 μl culture simultaneously caused a 2-fold dilution of the peptide, altering the peptide concentration range to 128 → 0.25 μg/ml.

Two control experiments were performed: a growth control was created by inoculating 5×10^5 cfu/ml of the culture in 100 μl of Mueller Hinton broth. A sterility control was created containing 100 μl of Mueller Hinton broth in the absence of peptide or culture. These plates were covered with other sterile polypropylene plates acting as lids to prevent contamination. These plates were incubated at 37 °C for 24 h. Growth was determined by measuring the absorbance at 600 nm for each well. The MIC for a given peptide and a given organism was the first peptide concentration that completely inhibited growth (reading along a peptide concentration range of 128 → 0.25 μg/ml).

Some organisms displayed mucoid or plaque morphologies, which made the estimation of growth through absorbance inaccurate. For such organisms, protocol E was modified to include resazurin (54, 55). Resazurin is a weak fluorescent dye that is irreversibly reduced to fluorescent resorufin in proportion to aerobic respiration. Using this modified protocol, cultures in 96-well polypropylene plates were incubated at 37 °C for 12 h. 30 μl of a 0.02% (w/v) aqueous resazurin solution was then pipetted into each well. Further incubation was performed at 37 °C for 12 h. Growth was estimated based on fluorescence measurements (excitation, 530 nm, and emission, 590 nm, reported as arbitrary fluorescence units). The percentage growth in each well was estimated based on Equation 3, and wells containing ≤5% growth were considered to display peptide bactericidal activity.

$$\%\_gth = \frac{\text{fluorescence} - \text{mean(sterility\_ctrl)}}{\text{mean}(gth\_\text{ctrl}) - \text{mean(sterility\_ctrl)}} \times 100 \quad \text{(Eq. 3)}$$

Cell culture and cytotoxicity assay

HeLa and HaCaT cells were grown in Dulbecco's modified Eagle's medium. The medium was supplemented with 10% fetal bovine serum, penicillin, streptomycin, and gentamycin. Cells were grown in serum-containing growth media until they reached 80–90% confluence. These cells were later used for the cytotoxicity assay.

The cytotoxicity of our peptides was evaluated using the MTT assay. Approximately 1×10^4 cells per well were seeded into polystyrene 96-well plates with 200 μl of medium. These plates were incubated at 37 °C for 12 h (5% CO_2), after which they were exposed to various concentrations of peptides and incubated at 37 °C for 24 h (5% CO_2). MTT was added to each well at a final concentration of 0.5 mg/ml. The plates were then incubated at 37 °C for 4 h (5% CO_2). After the supernatant was aspirated, 150 μl of dimethyl sulfoxide (DMSO) was added to each well and incubated at 37 °C for 10 min (5% CO_2). Absorbance measurements were performed at 570 nm using the Multi-Mode Microplate Reader (Biotek). Results were reported in the form of percentage growth, which was the growth of peptide-treated cells relative to untreated cells cultured under identical conditions. Five replicates for all peptide concentrations was performed, from which the mean percentage growth and standard deviation were calculated.

Peptide in vivo toxicity experiments using a mouse model

6–8-Week-old BALB/c mice (male and female) weighing ~20 g were used as *in vivo* models to determine peptide toxicity. Toxicity was determined by injecting peptide suspended in buffer (20% DMSO, 80% saline) intraperitoneally and monitoring all mice for 7 days while recording all deaths. Vehicle controls consisting of buffer-only injections were also performed. All mice were euthanized via ketamine overdose at the end of the experiment. LD_{50} values were then calculated using linear interpolation.

Blood tests (blood urea nitrogen and aspartate aminotransferase) and histopathological tests (hematoxylin-eosin staining of liver and kidney sections) were performed to determine the hepatotoxic and nephrotoxic properties of our peptides at therapeutic doses. Four cohorts of mice were used for these tests. Cohort 1 consisted of untreated BALB/c mice (female). Cohort 2 consisted of BALB/c mice (female) treated with a single dose

of 64 μg/g (35.57 μmol/g) NN2_0018 in buffer. Cohort 3 consisted of untreated BALB/c mice (male). Cohort 4 consisted of BALB/c mice (male) treated with a single dose of 64 μg/g (35.57 μmol/g) NN2_0018 in buffer. All mice were incubated for 24 h post-injection and anesthetized using a terminal dose of ketamine. Blood was extracted immediately via cardiac puncture, although liver and kidney tissue samples were extracted post mortem.

All mice were housed in the Central Animal Facility, IISc, with feed and water provided *ad libitum*. All animal experiments described in this work were approved by the Institutional Animal Ethics Committee, IISc (Project No. CAF/Ethics/550/2017).

Peptide in vivo efficacy experiments using a mouse peritoneal model of infection

Experiments studying the peritoneal cfu clearance abilities of NN2_0018 were performed using 6–8-week-old BALB/c mice (female) weighing ~20 g infected with *A. baumannii* (P1270). A glycerol stock of *A. baumannii* (P1270) stored at −80 °C was thawed and inoculated into 10 ml of MH broth with 8 μg/ml (20.86 μM) meropenem to preserve the carbapenem-resistant phenotype. This culture was incubated at 37 °C/24 h. This culture was diluted to 1.5×10^8 cfu in saline using a McFarland 0.5 standard and was further diluted in saline to a final concentration of 1.85×10^7 cfu/ml. cfu counts were retrospectively confirmed by plating and colony counting. 200 μl of this suspension (3.7×10^6 cfu) was peritoneally injected into four cohorts of BALB/c mice containing eight mice per cohort. A description of the experiments performed on each cohort is provided in Fig. 4.

Mice were euthanized using a CO_2 overdose. Peritoneal washes were performed by injecting 5 ml of chilled saline into the peritoneum and gently massaging and extracting the peritoneal fluid. Serial dilutions in saline and plating in Mueller-Hinton agar containing 8 μg/ml (20.86 μM) meropenem was performed immediately. Colony counting was then performed to calculate peritoneal cfu loads.

For the duration of all experiments, mice were housed in the Central Animal Facility (CAF, IISc), and they were provided with pellet feed and water *ad libitum*.

SEM experiments

A 1-ml bacterial culture was incubated overnight at 37 °C/180 rpm in Mueller Hinton broth and then centrifuged at 6000 rpm for 10 min. The pellet was resuspended in sterile phosphate-buffered saline (PBS), and the A_{600} was adjusted to 0.3–0.4. This resuspension was divided into two 500-μl aliquots (test/control). Peptide was added to the test aliquot at a final concentration of 128 μg/ml. The control aliquot did not contain any peptide. Both aliquots were incubated at 37 °C for 2 h/180 rpm, then centrifuged at 6000 rpm for 10 min, and resuspended in 25 μl of PBS. 10 μl of each resuspension was pipetted onto a clean glass coverslip and air dried for 1 h. Air-dried samples were immersed in a 2.5% (w/v) glutaraldehyde solution made in PBS and incubated for 24 h under ambient conditions. Postincubation, these samples were washed three times with distilled water to remove traces of glutaraldehyde. Samples were immersed in 30, 50, 75, 85, 95, and 100% alcohol/water gradients for 3 min each for dehydration. The sample was dried in a hot-air oven at 70 °C for 4 h. A 10-nm gold coating was applied to the sample (attached to an aluminum stub) using the Quorum Q150R ES sputter coater. SEM experiments were performed using the Carl Zeiss Ultra 55 field emission scanning electron microscope (FESEM, mono). Samples were analyzed using an extra-high tension voltage of 5 kV and using magnifications ranging from ×10,000 to 50,000.

Generation of bacterial protoplasts

S. hemolyticus protoplasts were generated using a standard protocol (36). Briefly, *S. hemolyticus* was inoculated into 10 ml of Mueller Hinton broth and incubated overnight at 37 °C/180 rpm (culture A). 3 ml of this culture was directly inoculated into 10 ml of Mueller Hinton broth containing 5% sucrose, 0.1% $MgSO_4$, and 100 units/ml benzylpenicillin. This culture was incubated at 37 °C for 2 h/180 rpm (culture B). Protoplast generation was confirmed by Gram staining culture A and culture B. Untreated culture A was expected to stain Gram-positive. Treated culture B, lacking a cell wall, was expected to stain Gram-negative.

Confocal microscopy experiments

Fluorescence confocal microscopy experiments were performed to determine the subcellular localization of peptides NN2_0018 and NN2_0050. N-terminal FITC linkages were created for both peptides. DAPI and Nile red were used as counterstains. Briefly, the protocol is as follows. Stock solutions of DAPI (1 mg/ml in 5% 1,4-diazabicyclo[2.2.2]octane, 50% glycerol buffer), Nile red (2 mg/ml in acetone), and FITC-labeled peptide (2 mg/ml aqueous solution) were prepared beforehand. The culture chosen for experimentation was inoculated into 10 ml of Mueller Hinton broth and incubated at 37 °C for 12 h/180 rpm. 200 μl of this culture was diluted with 800 μl of sterile PBS. 1 μl of DAPI, 1 μl of Nile red, and 4 μl of FITC-labeled peptide were added to the culture. Vortexing and centrifugation at 10,000 rpm for 1 min was performed immediately. The pellet was resuspended in 200 μl of sterile PBS. 5 μl of this suspension was pipetted onto a clean glass slide, sealed with a clean coverslip, and visualized using the Zeiss Observer Z.1 confocal microscope. DAPI, green fluorescent protein (GFP), and DSRed2 standard filters were used for fluorescence experiments. Images were captured using the AxioVision Release 4.8.2 SP2 (08-2013) software. All images were captured using a ×63 oil immersion objective. We attempted to minimize the total time interval between the introduction of stains and image acquisition. All images were captured <10 min after the introduction of fluorescent stains.

All images were acquired in the .png format, where the red/green/blue (R/G/B) channels were used to separately store intensity values for each stain. For clarity, representative regions of all images were selected and digitally magnified by ×3. Quantification of stain colocalization was performed using Pearson's correlation. Initially, K-means clustering was performed to partition pixels into two clusters. The cluster corresponding to the lower mean was considered to include the background and was ignored. For the R/G (Nile red/FITC-peptide), G/B (FITC-peptide/DAPI), and R/B (Nile-red/DAPI)

channels, pixel-intensity values were compared using Pearson's correlation. Higher correlation values were considered to represent better stain colocalization. Python scripts for image analysis are provided in Dataset S2.

Preparation of samples for microarray analysis

A carbapenem-resistant clinical *E. coli* isolate (P1645ec) was chosen for differential gene expression experiments upon exposure to peptide NN2_0018. Two replicates of *E. coli* (P1645ec) were incubated at 37 °C/24 h in 10 ml of MH media, supplemented with NN2_0018 at half-MBC concentrations (4 μg/ml, 2.22 μM). Two control replicates of *E. coli* (P1645ec) incubated at 37 °C/24 h in 10 ml of MH media, but without NN2_0018, were also grown. All four samples were also supplemented with 8 μg/ml (20.86 μM) meropenem to maintain their carbapenem-resistant phenotype. After incubation, all four samples were centrifuged at 6000 rpm for 10 min, and the pellets were flash-frozen using liquid nitrogen. RNA extraction, quality control, and *E. coli* microarray mRNA hybridization experiments using an Agilent CGH platform were performed by Genotypic, India, using an *E. coli* 8 × 15,000 array.

Functional gene set enrichment analysis

Microarray data preprocessing was performed in R, using the limma package available through Bioconductor. The median signal and background intensities were extracted using the read.maimages() function (56). Signal intensities were background-adjusted using the normexp() function (56). Background-adjusted signals were then log2-transformed and quantile-normalized to make the intensities consistent across each array (56).

Differential analysis was performed for NN2_0018-treated *E. coli* (P1645ec) with respect to an untreated *E. coli* control. Genes with a 1.319 ($2^{0.4}$)-fold change (up/down-regulation) and with a false discovery rate (FDR)-corrected *p* value calculated using the Benjamini and Hochberg method (57) less than or equal to 0.05 were considered as significantly differentially expressed genes (DEGs). This analysis revealed a significant up-regulation of 145 genes and a significant down-regulation of 26 genes. These DEGs were considered for downstream functional enrichment analysis through classification into functional groups using ClueGO comprehensive enrichment analysis.

ClueGO 2.2.5 (58) is a Cytoscape3.2 plugin. ClueGO attempts to classify genes into different functional groups. For example, genes occurring in the same metabolic pathways, the same subcellular locations, or acting upon the same substrate/product would be classified under the same functional group. ClueGO functional groups are composed of 3023 biological processes, 280 cellular components, 2591 molecular functions, and 105 pathway resources derived from the Kyoto Encyclopedia of Genes and Genomes (KEGG) (59). Cluego further integrates a list of identified gene ontology (GO) terms and pathways and organizes them into functionally grouped networks. These networks depict the biological relationship between the pathways and gene ontologies. ClueGO possessed sufficient information for 111 genes of the 145 up-regulated genes previously described. Further pruning to remove redundancy resulted in a list of 79 genes. Similarly, ClueGO possessed sufficient information for 20 genes of the 26 down-regulated genes previously described. Further pruning to remove redundancy resulted in a list of 14 genes.

To infer statistically significant functional groups, we used two-sided (enrichment/depletion) hyper-geometric distribution tests, with an FDR-corrected *p* value ≤0.05 using Bonferroni adjustment for the terms and the groups created by ClueGO. To reduce redundancy in the GO term categories, fusion option was performed with κ score set to 0.4. Further redundancy was manually identified and corrected.

Circular dichroism experiments

The Jasco J-810 spectrophotometer was used to perform all circular dichroism (CD) experiments. Samples were loaded into a quartz cuvette with a sample volume of 300 μl and a path length of 1 mm. Far-ultraviolet spectra were collected at a wavelength range of 200–250 nm. All spectra were collected at a 3-nm bandwidth and a 4-s response time. All spectra were collected three times, averaged, and corrected for buffer spectrum.

NMR experiments

NMR spectra were collected on the Agilent 600-MHz spectrometer using a triple-resonance z-gradient cryogenic probe. DPC (D38) micelles were used as a membrane-mimicking co-solvent. 1 mM peptide was suspended in excess DPC (15 mM DPC in 90% H_2O/10% D_2O; 15:1 DPC/peptide ratio) for all experiments. 1D ^{1}H NMR spectrum was acquired with 16,384 complex points and 64 scans. ^{1}H,^{1}H-NOESY (nuclear Overhauser effect spectroscopy) spectrum was acquired with 4096 complex points in the directly acquired dimension and 1024 complex points in the indirectly acquired dimension, and 32 scans. The spectra were processed with the program NMRPipe (60).

Author contributions—D. N. designed, performed, and analyzed experiments (Figs. 2*A*, 2*C–F*, 3–6, 8, and 9*A* and Tables 1–5). T. N. designed the LSTM algorithm (Fig. 1). N. R. designed, performed, and analyzed all NMR experiments (Fig. 9, *B–D*). O. K. co-performed all mouse *in vivo* experiments (Figs. 2, *C–F*, 3, and 4). SR analyzed *E. coli* (P1645ec) microarray data (Fig. 7 and Table 5). M. M. designed, performed, and analyzed HeLa cell line toxicity experiments (Fig. 2*B*). D. C. coordinated the study, planned experiments, and provided resources. N. C. coordinated the study, planned experiments, and provided resources. All authors reviewed the results and approved the final version of the manuscript.

Acknowledgments—We thank Dr. V. A. Indumathi and Dr. T. Sandeep from MS Ramaiah Medical College for providing clinical isolates from their culture collection. We thank Satya Tapas for significant logistical contributions. We thank Prof. Anjali Karande for providing the HeLa cell line. NMR experiments were analyzed by Prof. Siddhartha P. Sarma, and we thank him for the same. We thank the Central Animal Facility (IISc) for providing the large number of animals required for this work. We thank the Micro Nano Characterization Facility (MNCF) facility (Centre for Nano Science and Engineering (CeNSE), IISc) for SE access. We thank the Department of Science and Technology (DST, India) for the NMR facilities at IISc.

References

1. O'Neill, J. (2014) Antimicrobial Resistance: Tackling a Crisis for the Health and Wealth of Nations. Review on Antimicrobial Resistance. London, UK
2. Peschel, A., and Sahl, H.-G. (2006) The co-evolution of host cationic antimicrobial peptides and microbial resistance. *Nat. Rev. Microbiol.* **4,** 529–536 CrossRef Medline
3. Ge, Y., MacDonald, D. L., Holroyd, K. J., Thornsberry, C., Wexler, H., and Zasloff, M. (1999) *In vitro* antibacterial properties of pexiganan, an analog of magainin. *Antimicrob. Agents Chemother.* **43,** 782–788 Medline
4. Sader, H. S., Fedler, K. A., Rennie, R. P., Stevens, S., and Jones, R. N. (2004) Omiganan pentahydrochloride (mbi 226), a topical 12-amino-acid cationic peptide: spectrum of antimicrobial activity and measurements of bactericidal activity. *Antimicrob. Agents Chemother.* **48,** 3112–3118 CrossRef Medline
5. Nell, M. J., Tjabringa, G. S., Wafelman, A. R., Verrijk, R., Hiemstra, P. S., Drijfhout, J. W., and Grote, J. J. (2006) Development of novel ll-37 derived antimicrobial peptides with lps and lta neutralizing and antimicrobial activities for therapeutic application. *Peptides* **27,** 649–660 CrossRef Medline
6. Fox, J. L. (2013) Antimicrobial peptides stage a comeback. *Nat. Biotechnol.* **31,** 379–382 CrossRef Medline
7. Namjoshi, S., and Benson, H. A. (2010) Cyclic peptides as potential therapeutic agents for skin disorders. *Biopolymers* **94,** 673–680 CrossRef Medline
8. Saravolatz, L. D., Pawlak, J., Johnson, L., Bonilla, H., Saravolatz, L. D., 2nd., Fakih, M. G., Fugelli, A., and Olsen, W. M. (2012) *In vitro* activities of ltx-109, a synthetic antimicrobial peptide, against methicillin-resistant, vancomycin-intermediate, vancomycin-resistant, daptomycin-nonsusceptible, and linezolid-nonsusceptible *Staphylococcus aureus*. *Antimicrob. Agents Chemother.* **56,** 4478–4482 CrossRef Medline
9. Piotto, S. P., Sessa, L., Concilio, S., and Iannelli, P. (2012) Yadamp: yet another database of antimicrobial peptides. *Int. J. Antimicrob. Agents* **39,** 346–351 CrossRef Medline
10. Wang, Z., and Wang, G. (2004) Apd: the antimicrobial peptide database. *Nucleic Acids Res.* **32,** D590–D592 CrossRef Medline
11. Thomas, S., Karnik, S., Barai, R. S., Jayaraman, V. K., and Idicula-Thomas, S. (2009) Camp: a useful resource for research on antimicrobial peptides. *Nucleic Acids Res.* **38,** D770–D780 Medline
12. Matsuzaki, K., Murase, O., Fujii, N., and Miyajima, K. (1996) An antimicrobial peptide, magainin 2, induced rapid flip-flop of phospholipids coupled with pore formation and peptide translocation. *Biochemistry* **35,** 11361–11368 CrossRef Medline
13. Shai, Y. (2002) Mode of action of membrane active antimicrobial peptides. *Biopolymers* **66,** 236–248 CrossRef Medline
14. Baumann, G., and Mueller, P. (1974) A molecular model of membrane excitability. *J. Supramol. Struct.* **2,** 538–557 CrossRef Medline
15. Brogden, K. A. (2005) Antimicrobial peptides: pore formers or metabolic inhibitors in bacteria? *Nat. Rev. Microbiol.* **3,** 238–250 CrossRef Medline
16. Gusman, H., Travis, J., Helmerhorst, E. J., Potempa, J., Troxler, R. F., and Oppenheim, F. G. (2001) Salivary histatin 5 is an inhibitor of both host and bacterial enzymes implicated in periodontal disease. *Infect. Immun.* **69,** 1402–1408 CrossRef Medline
17. Yonezawa, A., Kuwahara, J., Fujii, N., and Sugiura, Y. (1992) Binding of tachyplesin I to dna revealed by footprinting analysis: significant contribution of secondary structure to DNA binding and implication for biological action. *Biochemistry* **31,** 2998–3004 CrossRef Medline
18. Subbalakshmi, C., and Sitaram, N. (1998) Mechanism of antimicrobial action of indolicidin. *FEMS Microbiol. Lett.* **160,** 91–96 CrossRef Medline
19. Patrzykat, A., Friedrich, C. L., Zhang, L., Mendoza, V., and Hancock, R. E. (2002) Sublethal concentrations of pleurocidin-derived antimicrobial peptides inhibit macromolecular synthesis in *Escherichia coli*. *Antimicrob. Agents Chemother.* **46,** 605–614 CrossRef Medline
20. Sass, P., Jansen, A., Szekat, C., Sass, V., Sahl, H.-G., and Bierbaum, G. (2008) The lantibiotic mersacidin is a strong inducer of the cell wall stress response of *Staphylococcus aureus*. *BMC Microbiol.* **8,** 186 CrossRef Medline
21. Friedrich, C. L., Moyles, D., Beveridge, T. J., and Hancock, R. E. (2000) Antibacterial action of structurally diverse cationic peptides on Gram-positive bacteria. *Antimicrob. Agents Chemother.* **44,** 2086–2092 CrossRef Medline
22. Wenzel, M., Chiriac, A. I., Otto, A., Zweytick, D., May, C., Schumacher, C., Gust, R., Albada, H. B., Penkova, M., Krämer, U., Erdmann, R., Metzler-Nolte, N., Straus, S. K., Bremer, E., Becher, D., *et al.* (2014) Small cationic antimicrobial peptides delocalize peripheral membrane proteins. *Proc. Natl. Acad. Sci.* **111,** E1409–E1418 CrossRef Medline
23. Blondelle, S. E., and Houghten, R. A. (1992) Design of model amphipathic peptides having potent antimicrobial activities. *Biochemistry* **31,** 12688–12694 CrossRef Medline
24. Deslouches, B., Phadke, S. M., Lazarevic, V., Cascio, M., Islam, K., Montelaro, R. C., and Mietzner, T. A. (2005) *De novo* generation of cationic antimicrobial peptides: influence of length and tryptophan substitution on antimicrobial activity. *Antimicrob. Agents Chemother.* **49,** 316–322 CrossRef Medline
25. Deslouches, B., Steckbeck, J. D., Craigo, J. K., Doi, Y., Mietzner, T. A., and Montelaro, R. C. (2013) Rational design of engineered cationic antimicrobial peptides consisting exclusively of arginine and tryptophan, and their activity against multidrug-resistant pathogens. *Antimicrob. Agents Chemother.* **57,** 2511–2521 CrossRef Medline
26. Lam, S. J., O'Brien-Simpson, N. M., Pantarat, N., Sulistio, A., Wong, E. H., Chen, Y.-Y., Lenzo, J. C., Holden, J. A., Blencowe, A., Reynolds, E. C., and Qiao, G. G. (2016) Combating multidrug-resistant Gram-negative bacteria with structurally nanoengineered antimicrobial peptide polymers. *Nat. Microbiol.* **1,** 16162 CrossRef Medline
27. Fjell, C. D., Jenssen, H., Cheung, W. A., Hancock, R. E., and Cherkasov, A. (2011) Optimization of antibacterial peptides by genetic algorithms and cheminformatics. *Chem. Biol. Drug Des.* **77,** 48–56 CrossRef Medline
28. Loose, C., Jensen, K., Rigoutsos, I., and Stephanopoulos, G. (2006) A linguistic model for the rational design of antimicrobial peptides. *Nature* **443,** 867–869 CrossRef Medline
29. Maccari, G., Di Luca, M., Nifosí, R., Cardarelli, F., Signore, G., Boccardi, C., and Bifone, A. (2013) Antimicrobial peptides design by evolutionary multiobjective optimization. *PLoS Comput. Biol.* **9,** e1003212 CrossRef Medline
30. Hochreiter, S., and Schmidhuber, J. (1997) Long short-term memory. *Neural Comput.* **9,** 1735–1780 CrossRef Medline
31. Thompson, J. D., Gibson, T., and Higgins, D. G. (2002) Multiple sequence alignment using ClustalW and ClustalX. *Curr. Protoc. Bioinformatics* Chapter 2, Unit 2.3 Medline
32. Wiegand, I., Hilpert, K., and Hancock, R. E. (2008) Agar and broth dilution methods to determine the minimal inhibitory concentration (mic) of antimicrobial substances. *Nat. Protoc.* **3,** 163–175 CrossRef Medline
33. Dai, C., Li, J., Tang, S., Li, J., and Xiao, X. (2014) Colistin-induced nephrotoxicity in mice involves the mitochondrial, death receptor, and endoplasmic reticulum pathways. *Antimicrob. Agents Chemother.* **58,** 4075–4085 CrossRef Medline
34. Keirstead, N. D., Wagoner, M. P., Bentley, P., Blais, M., Brown, C., Cheatham, L., Ciaccio, P., Dragan, Y., Ferguson, D., Fikes, J., Galvin, M., Gupta, A., Hale, M., Johnson, N., Luo, W., *et al.* (2013) Early prediction of polymyxin-induced nephrotoxicity with next-generation urinary kidney injury biomarkers. *Toxicol. Sci.* **137,** 278–291 Medline
35. Deleted in proof
36. Lederberg, J. (1956) Bacterial protoplasts induced by penicillin. *Proc. Natl. Acad. Sci. U.S.A.* **42,** 574–577 CrossRef Medline
37. Lamarche, M. G., Wanner, B. L., Crépin, S., and Harel, J. (2008) The phosphate regulon and bacterial virulence: a regulatory network connecting phosphate homeostasis and pathogenesis. *FEMS Microbiol. Rev.* **32,** 461–473 CrossRef Medline
38. Smith, R. S., Wolfgang, M. C., and Lory, S. (2004) An adenylate cyclase-controlled signaling network regulates *Pseudomonas aeruginosa* virulence in a mouse model of acute pneumonia. *Infect. Immun.* **72,** 1677–1684 CrossRef Medline
39. Carbonetti, N. H., Artamonova, G. V., Andreasen, C., and Bushar, N. (2005) Pertussis toxin and adenylate cyclase toxin provide a one-two punch for establishment of *Bordetella pertussis* infection of the respiratory tract. *Infect. Immun.* **73,** 2698–2703 CrossRef Medline

40. Laoide, B. M., and Ullmann, A. (1990) Virulence dependent and independent regulation of the *Bordetella pertussis* cya operon. *EMBO J.* **9,** 999–1005 Medline
41. Stonehouse, E., Kovacikova, G., Taylor, R. K., and Skorupski, K. (2008) Integration host factor positively regulates virulence gene expression in *Vibrio cholerae*. *J. Bacteriol.* **190,** 4736–4748 CrossRef Medline
42. Mangan, M. W., Lucchini, S., Danino, V., Cróinín, T. O., Hinton, J. C., Dorman, C. J. (2006) The integration host factor (ihf) integrates stationary-phase and virulence gene expression in *Salmonella enterica* serovar *typhimurium*. *Mol. Microbiol.* **59,** 1831–1847 CrossRef Medline
43. Chong, Z.-S., Woo, W.-F., and Chng, S.-S. (2015) Osmoporin ompc forms a complex with mlaa to maintain outer membrane lipid asymmetry in *Escherichia coli*. *Mol. Microbiol.* **98,** 1133–1146 CrossRef Medline
44. Chen, Y. Y., and Gänzle, M. G. (2016) Influence of cyclopropane fatty acids on heat, high pressure, acid and oxidative resistance in *Escherichia coli*. *Int. J. Food Microbiol.* **222,** 16–22 CrossRef Medline
45. Cullen, J., Phillips, M. C., and Shipley, G. G. (1971) The effects of temperature on the composition and physical properties of the lipids of *Pseudomonas fluorescens*. *Biochem. J.* **125,** 733–742 CrossRef Medline
46. Moss, R. A., Fujita, T., Okumura, Y., Hua, Z., Mendelsohn, R., and Senak, L. (1992) Comparative dynamic stabilities of cyclopropyl and olefinic model lipids in liposomes. A coordinated kinetic and spectroscopic study. *Langmuir* **8,** 1731–1735 CrossRef
47. Loffhagen, N., Härtig, C., Geyer, W., Voyevoda, M., and Harms, H. (2007) Competition between cis, trans and cyclopropane fatty acid formation and its impact on membrane fluidity. *Eng. Life Sci.* **7,** 67–74 CrossRef
48. Loiseau, L., Gerez, C., Bekker, M., Ollagnier-de Choudens, S., Py, B., Sanakis, Y., Teixeira de Mattos, J., Fontecave, M., and Barras, F. (2007) Erpa, an iron–sulfur (Fe–S) protein of the a-type essential for respiratory metabolism in *Escherichia coli*. *Proc. Natl. Acad. Sci. U.S.A.* **104,** 13626–13631 CrossRef Medline
49. Miller, M. J., and Gennis, R. (1983) The purification and characterization of the cytochrome *d* terminal oxidase complex of the *Escherichia coli* aerobic respiratory chain. *J. Biol. Chem.* **258,** 9159–9165 Medline
50. Tielens, A. G., and Van Hellemond, J. J. (1998) The electron transport chain in anaerobically functioning eukaryotes. *Biochim. Biophys. Acta* **1365,** 71–78 CrossRef Medline
51. Katsu, T., Ninomiya, C., Kuroko, M., Kobayashi, H., Hirota, T., and Fujita, Y. (1988) Action mechanism of amphipathic peptides gramicidin s and melittin on erythrocyte membrane. *Biochim. Biophys. Acta* **939,** 57–63 CrossRef Medline
52. World Health Organization (2017) Global priority list of antibiotic-resistant bacteria to guide research, discovery, and development of new antibiotics. World Health Organization, Geneva, Switzerland (http://www.who.int/medicines/publications/WHO-PPL-Short_Summary_25Feb-ET_NM_WHO.pdf)
53. Kozlowska, J., Vermeer, L. S., Rogers, G. B., Rehnnuma, N., Amos, S.-B., Koller, G., McArthur, M., Bruce, K. D., and Mason, A. J. (2014) Combined systems approaches reveal highly plastic responses to antimicrobial peptide challenge in *Escherichia coli*. *PLoS Pathog.* **10,** e1004104 CrossRef Medline
54. Sarker, S. D., Nahar, L., and Kumarasamy, Y. (2007) Microtitre plate-based antibacterial assay incorporating resazurin as an indicator of cell growth, and its application in the *in vitro* antibacterial screening of phytochemicals. *Methods* **42,** 321–324 CrossRef Medline
55. 55 Deleted in proof
56. 56 Smyth, G. (2005) *Limma: linear models for microarray data*. *Bioinforma. Computational Biology Solutions Using R Bioconductor*, pp. 397–420, Springer, New York
57. 57 Benjamini, Y., and Hochberg, Y. (1995) Controlling the false discovery rate: a practical and powerful approach to multiple testing. *J. R. Stat. Soc. B*, 289–300
58. 58 Bindea, G., Mlecnik, B., Hackl, H., Charoentong, P., Tosolini, M., Kirilovsky, A., Fridman, W.-H., Pagès, F., Trajanoski, Z., and Galon, J. (2009) Cluego: a cytoscape plug-in to decipher functionally grouped gene ontology and pathway annotation networks. *Bioinformatics* **25,** 1091–1093 CrossRef Medline
59. 59 Kanehisa, M., and Goto, S. (2000) KEGG: Kyoto encyclopedia of genes and genomes. *Nucleic Acids Res.* **28,** 27–30 CrossRef Medline
60. 60 Delaglio, F., Grzesiek, S., Vuister, G. W., Zhu, G., Pfeifer, J., and Bax, A. (1995) Nmrpipe: a multidimensional spectral processing system based on unix pipes. *J. Biomol. NMR* **6,** 277–293 Medline